

DESIGN AND DEVELOPMENT OF A DISTRIBUTED CONTROL SCHEME
FOR AN AC STACKED DISTRIBUTED PV INVERTER ARCHITECTURE

by

Saurabh B. Trivedi

A thesis submitted to the faculty of
The University of North Carolina at Charlotte
in partial fulfillment of the requirements
for the degree of Master of Science in
Electrical Engineering

Charlotte

2015

Approved by:

Dr. Babak Parkhideh

Dr. Robert Cox

Dr. Asis Nasipuri

© 2015
Saurabh B. Trivedi
ALL RIGHTS RESERVED

ABSTRACT

SAURABH B. TRIVEDI. Design and development of a distributed control scheme for an AC stacked distributed PV inverter architecture.
(Under the direction of DR. BABAK PARKHIDEH)

The increasing importance of renewable electricity, especially PV generation, and the reducing costs of PV modules has placed the inverter in limelight. Panel-level inverter configurations like Micro-inverter are gaining commercial importance, but hold a minor market share. On the other hand, PV inverters which are connected in series on the AC side, like cascaded multilevel inverter or cascaded H-bridge (CHB), are gaining research importance. Another such configuration called Inverter MoleculeTM(IM), which is at its nascent stage seems to be very promising as a panel-level inverter configuration.

The control structures employed for the distributed panel-level inverters in cascade such as CHB, are either centralized or hybrid. A control structure which is truly distributed, taking advantage of the inverter configuration/architecture, has not yet been developed. The hypothesis here is that, individual inverters of a string can be controlled independently of each other, without any communication because the common string current inherently shares the information with all members.

Hence, a novel distributed control scheme has been designed and developed and its feasibility for the IM architecture is proved in this thesis, by mathematical modeling and analysis, and simulation results.

DEDICATION

This thesis is dedicated to my dear parents, Bharat and Ila Trivedi, and my brother Bhavin Trivedi.

ACKNOWLEDGMENTS

Firstly, I would like to thank my teacher and mentor, Dr. Babak Parkhideh, who introduced me to power electronics and controls and provided continuous encouragement and support throughout the process.

I would like to thank Dr. Robert Cox and Dr. Asis Nasipuri for graciously accepting to serve on my thesis committee.

I would like to thank Dr. Shibashis Bhowmik (CEO and President of SineWatts, Inc.) for his support. I would also like to thank my colleagues and fellow research students, of Dr. Parkhideh's team and SineWatts' team, especially Hamidreza Jafarian, for taking up my share of work while I was busy with my thesis and also introducing me to many control related aspects of power electronics.

I would like to thank my family and my girlfriend, Mitali Shah, for their constant moral support.

Lastly, I would like to thank my roommates, friends and seniors at UNC Charlotte for being there for me.

This work and any subject invention is part of activities being performed under the US Department of Energy (DoE), SunShot Incubator Program, Incubator Round(s) 8 and 9. The information, data, or work presented herein was funded in part by the Office of Energy Efficiency and Renewable Energy (EERE), U.S. Department of Energy, under Award Number(s) DE-EE0006459 and DE-0006692.

DISCLAIMER

The information, data, or work presented herein was funded in part by an agency of the United States Government. Neither the United States Government nor any agency thereof, nor any of their employees, makes any warranty, express or implied, or assumes any legal liability or responsibility for the accuracy, completeness, or usefulness of any information, apparatus, product, or process disclosed, or represents that its use would not infringe privately owned rights. Reference herein to any specific commercial product, process, or service by trade name, trademark, manufacturer, or otherwise does not necessarily constitute or imply its endorsement, recommendation, or favoring by the United States Government or any agency thereof. The views and opinions of authors expressed herein do not necessarily state or reflect those of the United States Government or any agency thereof.

TABLE OF CONTENTS

LIST OF FIGURES	ix
LIST OF TABLES	xii
CHAPTER 1: INTRODUCTION	1
1.1 Electricity Generation	1
1.2 Motivation	2
1.2.1 Renewable Electricity Challenges	2
1.2.2 Photovoltaic Inverter	3
1.3 Organization of Thesis	4
CHAPTER 2: BACKGROUND	5
2.1 Introduction	5
2.2 PV Inverter Configurations	5
2.3 Control Scheme	7
2.3.1 Voltage Controller	10
2.3.2 Current Controller	10
2.4 Cascaded Multilevel Inverters	13
2.4.1 Topology and Operation	13
2.4.2 Control Scheme	15
2.5 Inverter Molecule™	17
2.6 Conclusion	19
CHAPTER 3: MODELING, ANALYSIS AND CONTROLLER DESIGN	20
3.1 Introduction	20
3.2 Single Phase PV Inverter Modeling	20
3.3 Modeling and Analysis of IM	24
3.3.1 Modeling	24

	viii
3.3.2 Analysis	27
3.4 Feedback Control Design for IM	30
3.4.1 Formulation	30
3.4.2 Analytical Design	34
3.4.3 Asymmetric Operation Analysis	37
3.5 Conclusion	40
CHAPTER 4: SIMULATION AND RESULTS	43
4.1 Introduction	43
4.2 Simulation Setup	43
4.3 Simulation Results	47
4.3.1 Case 1: Symmetric Operation	47
4.3.2 Case 2: Shading on SM2	51
4.3.3 Case 3: Shading on SM1	55
4.3.4 Case 4: Grid Disturbance	59
CHAPTER 5: CONCLUSION	64
5.1 Summary	64
5.2 Future Work	65
REFERENCES	67

LIST OF FIGURES

FIGURE 1.1: Net electricity generation in the U.S. [1].	1
FIGURE 1.2: LCOE of PV systems [4].	3
FIGURE 2.1: Grid-tie PV inverter configurations: (a)Central inverter (b)String inverter (c)Multi-string inverter (d)Micro-inverter.	6
FIGURE 2.2: PV characteristics [7].	8
FIGURE 2.3: Single-stage grid-tie PV inverter control scheme.	9
FIGURE 2.4: Two-stage grid-tie PV inverter control scheme.	9
FIGURE 2.5: Relation between $\alpha\beta$ and D-Q frames.	12
FIGURE 2.6: D-Q controller.	12
FIGURE 2.7: Cascaded H-bridge topology.	14
FIGURE 2.8: Multilevel modulation techniques: (a)SHE PWM (b)Phase-shifted PWM [20].	14
FIGURE 2.9: Centralized control scheme for CHB.	15
FIGURE 2.10: Hybrid control scheme for CHB.	16
FIGURE 2.11: Distributed control scheme for IM.	18
FIGURE 3.1: Single phase inverter.	21
FIGURE 3.2: IM model.	25
FIGURE 3.3: State variable feedback system.	30
FIGURE 3.4: Step response of closed loop system.	38
FIGURE 3.5: Step response of closed loop system with asymmetric operating points.	41

FIGURE 3.6: IM system with controller.	42
FIGURE 4.1: Simulink model of IM with controller.	44
FIGURE 4.2: Simulink model of unipolar PWM generator.	45
FIGURE 4.3: Simulink model of peak current controller.	46
FIGURE 4.4: DC voltage and reference of SM1 for case 1: symmetrical ramping up to maximum power.	48
FIGURE 4.5: DC voltage and reference of SM2 for case 1: symmetrical ramping up to maximum power.	49
FIGURE 4.6: Grid voltage and current for case 1: symmetrical ramping up to maximum power.	49
FIGURE 4.7: Grid voltage and current at MPP steady-state for case 1: symmetrical ramping up to maximum power.	50
FIGURE 4.8: Grid current THD for case 1: symmetrical ramping up to maximum power.	50
FIGURE 4.9: Grid current THD at MPP steady-state for case 1: symmetrical ramping up to maximum power.	51
FIGURE 4.10: AC voltages of individual SMs for case 1: symmetrical ramping up to maximum power.	51
FIGURE 4.11: Power ramp-up for case 1: symmetrical ramping up to maximum power.	52
FIGURE 4.12: DC voltage and reference of SM1 for case 2: shading on SM2 at 0.9 s.	53
FIGURE 4.13: DC voltage and reference of SM2 for case 2: shading on SM2 at 0.9 s.	53
FIGURE 4.14: Grid voltage and current for case 2: shading on SM2 at 0.9 s.	54
FIGURE 4.15: Grid current THD for case 2: shading on SM2 at 0.9 s.	54
FIGURE 4.16: AC voltages of individual SMs for case 2: shading on SM2 at 0.9 s.	55

FIGURE 4.17: DC and AC power for case 2: shading on SM2 at 0.9 s.	56
FIGURE 4.18: DC voltage and reference of SM1 for case 3: shading on SM1 at 0.9 s.	56
FIGURE 4.19: DC voltage and reference of SM2 for case 3: shading on SM1 at 0.9 s.	57
FIGURE 4.20: Grid voltage and current for case 3: shading on SM1 at 0.9 s.	57
FIGURE 4.21: Grid current THD for case 3: shading on SM1 at 0.9 s.	58
FIGURE 4.22: AC voltages of individual SMs for case 3: shading on SM1 at 0.9 s.	58
FIGURE 4.23: DC and AC power for case 3: shading on SM1 at 0.9 s.	59
FIGURE 4.24: Grid voltage and current for case 4: grid disturbance - 10% at 0.9 s and 18.18% at 1.2 s.	60
FIGURE 4.25: AC voltages of individual SMs for case 4: grid disturbance - 10% at 0.9 s and 18.18% at 1.2 s.	60
FIGURE 4.26: DC voltage and reference of SM1 for case 4: grid disturbance - 10% at 0.9 s and 18.18% at 1.2 s.	61
FIGURE 4.27: DC voltage and reference of SM2 for case 4: grid disturbance - 10% at 0.9 s and 18.18% at 1.2 s.	61
FIGURE 4.28: DC and AC power for case 4: grid disturbance - 10% at 0.9 s and 18.18% at 1.2 s.	62
FIGURE 4.29: Grid current THD for case 4: grid disturbance - 10% at 0.9 s and 18.18% at 1.2 s.	63

LIST OF TABLES

TABLE 3.1: Nominal operating points.	29
TABLE 3.2: Asymmetric operating points.	39
TABLE 4.1: Physical parameters of simulink model.	47
TABLE 4.2: Controller parameters of simulink model.	47

CHAPTER 1: INTRODUCTION

1.1 Electricity Generation

Electricity generation has been largely dependent on sources of energy that are non-renewable, like fossil fuels and nuclear energy. Based on the data from EIA [1], as shown in Figure 1.1, the contribution of fossil fuels (coal and natural gas combined), nuclear and hydro-electric sources has not increased significantly since 2001, while the contribution of other renewable sources has increased by around 300%. But, generation from these renewable sources is still minor (approximately 7%) compared to conventional sources. The problem with this distribution is that these conventional sources are hazardous to the environment because of the toxic emissions. In 2010 alone, approximately 2.3 billion metric tons of CO_2 was emitted as a result of coal and natural gas used in electricity generation [1]. These emissions are a major contributor to global warming. Also, because of their unprecedented use, fossil fuels are fast depleting.

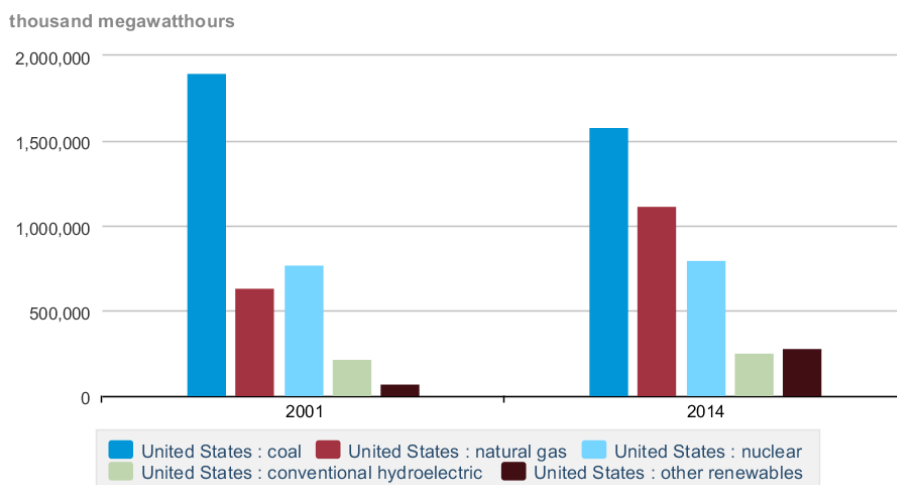


Figure 1.1: Net electricity generation in the U.S. [1].

Electricity generation from coal, natural gas, nuclear energy adds pollutants to traditional water resources, while producing electricity from geothermal energy may pollute ground water reserves in the process [2]. Hydro-electricity generation does not pollute water, but drastically changes the river habitats, due to dam construction. Thus, because of all the aforementioned reasons, the use of renewable sources like wind and solar in electricity generation must be encouraged as they have minimum negative impact on the environment.

1.2 Motivation

1.2.1 Renewable Electricity Challenges

There are many challenges involved in making renewable electricity mainstream and one of the biggest is the cost involved. The U.S. DOE's EERE office has been introducing a lot of programs to make renewable electricity cost-competitive compared to traditional sources. One such program is the 'SunShot' initiative introduced in 2011, which aims at bringing the cost of a utility scale PV system to \$1/W (levelized cost of energy of \$0.06/kWh) by 2020. Of this, \$0.5/W is the cost of PV module, \$0.1/W is the cost of power electronics and \$0.4/W is the balance of system (BOS) [3]. After just three years into the program, the cost has reduced significantly, as seen in Figure 1.2. Most of the reduction in cost is from the PV module costs, thus making the inverter, hardware and BOS the major contributors. The inverter cost has also reduced, from 1.6 c/kWh to 1 c/kWh but, it is required to reduce it further to 6 c/kWh (equivalent to \$0.1/W), based on SunShot targets.

Another major challenge of integration of renewable sources with the electrical grid, is the intermittent nature of generation because wind and solar insolation vary significantly with time. This problem can be solved by better planning and operation of the grid as suggested by NREL in their report [5]. But, it is equally important to increase the efficiency and reliability of the power electronics to deal with this problem.



Figure 1.2: LCOE of PV systems [4].

1.2.2 Photovoltaic Inverter

In order to harness solar energy, there are two types of technologies available; one is Photovoltaics, which converts the light to DC electricity while the other uses concentrated solar power to produce heat. Of these, PV technology is more widely used to generate electricity. But, as most of the transmission and distribution systems for delivering electricity use AC, the power conversion stage called ‘Inverter’ is necessary.

Traditionally, a central inverter configuration has been used, in which PV panels are connected together in series and parallel to build up the power, followed by the inverter stage connecting it to grid. This architecture, however, is not able to capture all the energy because variation in insolation on some PV modules affects the power extracted from others. This drawback has been overcome with newer architectures like the Micro-inverter, which is connected to a panel. But, this newer technology has disadvantages in terms of cost. Thus, there is a need for a better inverter configuration that can achieve panel-level optimization and also the cost targets set by DOE.

This thesis investigates a new configuration/architecture, based on an embodiment of [6], called Inverter Molecule™(IM), in which PV inverters, at panel-level, are con-

nected in series on the AC side to build up the voltage, and then connected to the grid. This configuration - an AC stacked distributed PV inverter, has the advantage of a micro-inverter and also reduced complexity and cost as each panel-level inverter is operating at lower voltage. It also provides benefits of higher efficiency and helps in reducing other hardware and BOS costs. Since, it is a new PV inverter architecture, this thesis aims at showing its feasibility with a distributed control scheme.

1.3 Organization of Thesis

A brief description of the reasons leading to the motivation of the thesis has been provided before. Remainder of the thesis is organized as follows:

Chapter 2 gives a background of PV inverter configurations/architectures that exist today and how they are controlled.

Chapter 3 derives the mathematical model of the IM architecture and gives the design and analysis of a distributed control scheme for it.

Chapter 4 discusses the results of the simulation of the IM configuration with the distributed control scheme, using MATLAB/Simulink.

Chapter 5 concludes the thesis and provides suggestions for future work.

CHAPTER 2: BACKGROUND

2.1 Introduction

In the introduction to this thesis, the importance of PV electricity and the prime role of the inverter was highlighted. This chapter will review different structure topologies (configurations) for grid connected PV inverters and their control structures. Section 2.2 introduces the commercially accepted PV inverter configurations like central inverter, string/multi-string inverter and the micro-inverter or AC module. Section 2.3 will introduce the control schemes that have been used for these inverter configurations. In the following section a more recent configuration called cascaded multilevel inverter and its control scheme is reviewed. Section 2.5 reviews a PV inverter technology which is in its nascent stage, called the Inverter MoleculeTM(IM) and its control method.

2.2 PV Inverter Configurations

The Central Inverter is the technology, in which a sufficient number of PV panels are connected in series such that the voltage built up is grid comparable, without need for boosting and such strings of panels are connected in parallel through diodes (to avoid damage to the modules by reverse flow of current) to build up the power (several kW), as shown in Figure 2.1(a) [7]. A central inverter is typically a 3-phase inverter but may also be single phase. Initially, it used line commutated thyristor bridge which injected current with high harmonic content and non-unity power factor into the grid, but, with advancement in power electronics, IGBTs, BJTs and MOSFETs have been used [8]. Typically, it is a single stage full-bridge with a power decoupling capacitor at the input and a filter network at the output. It may be coupled to the grid with

or without a transformer (at line frequency).

The advantages of central inverter are high efficiency and low cost per watt [8]. The disadvantages of this configuration are more evident: high voltage DC cables between the PV modules and inverter decrease safety, mismatch losses due to centralized MPPT or panel variations, losses in string diodes and non-flexible design [7], [8].

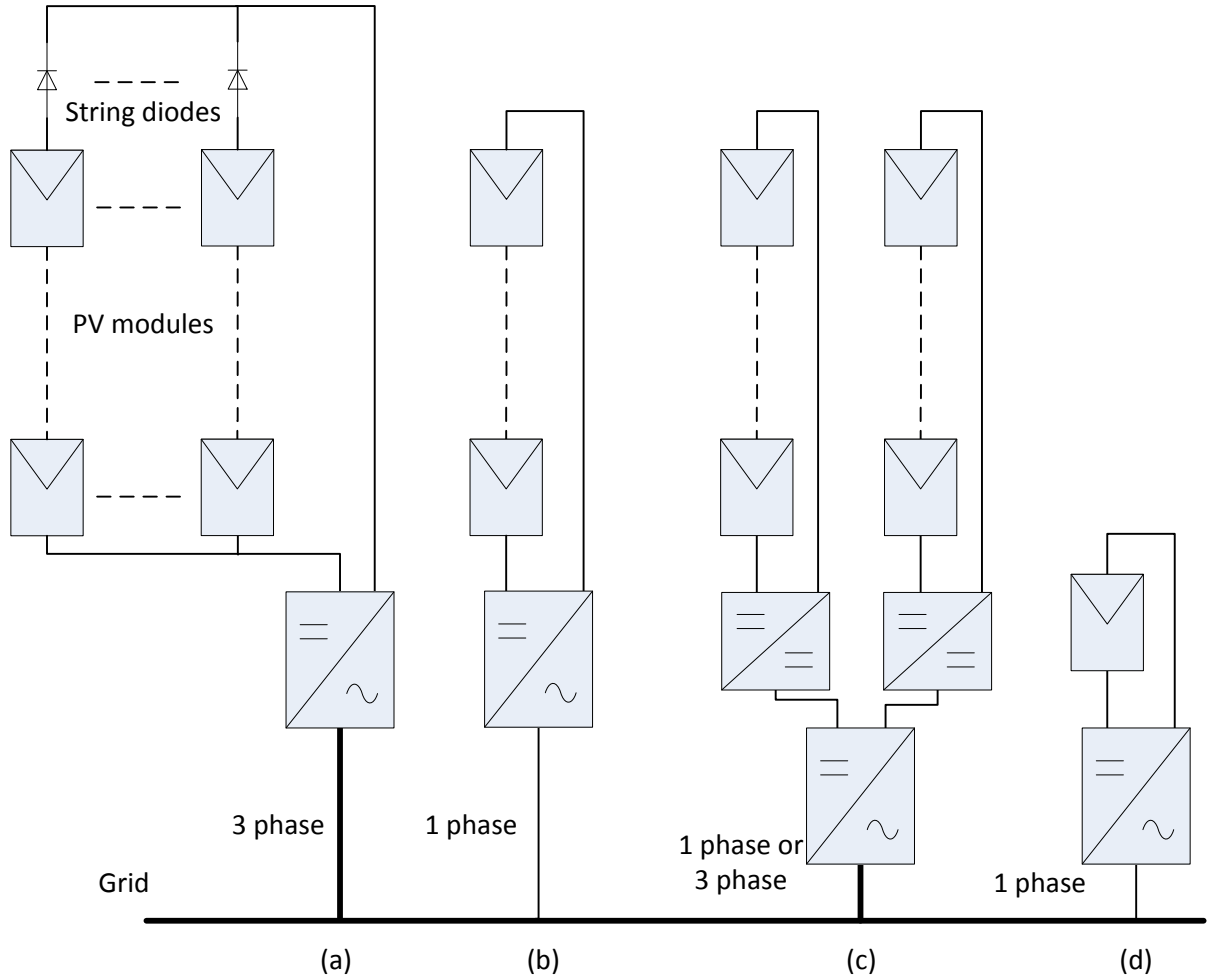


Figure 2.1: Grid-tie PV inverter configurations: (a)Central inverter (b)String inverter (c)Multi-string inverter (d)Micro-inverter.

String and multi-string inverters are the reduced versions of central inverter [9], shown in Figure 2.1(b) and (c). Instead of connecting the string of panels in parallel, they are directly connected to an inverter. This eliminates the diode losses. Also, the mismatch losses due to partial shading are reduced because each string MPP can be

controlled separately [7], [8], [9]. Similarly, in multi-string configuration, a DC-DC converter is employed for each string and the outputs of these converters are connected to a common DC bus followed by a central inverter. Both these configurations also have the advantage of being easily expandable, by adding a string with DC-DC optimizer or string inverter [7], [8], [9].

The AC module or micro-inverter consists of an inverter integrated with the PV module, thereby directly interfacing it to the grid, as shown in Figure 2.1(d). This configuration completely eliminates the mismatch losses as individual panel-level maximum power point tracking (MPPT) can be performed. Also, it provides the advantage of scaling up easily, owing to its modular structure. However, the main drawback is that it requires a boost stage in order to interface the panel-level voltage (25 V to 40 V) to grid voltage level. This, conversion is lossy and decreases the efficiency. Also, due to the complex power topologies involved, price per watt is higher [7], [9]. The advantages of micro-inverter make it the latest commercially accepted inverter technology for residential applications. But due to its disadvantages, it is not as widely accepted for PV power plants.

2.3 Control Scheme

Developing the control scheme for a particular PV inverter configuration is an essential task because both the input and output need to be controlled. Figure 2.2, shows the non-linear I-V and P-V characteristics of a PV module. Here, it is required to maintain the voltage at the output of PV as constant at the maximum power point (MPP). Thus, usually there is a power decoupling capacitor at the point of PV coupling to the power converter, whose voltage needs to be controlled. The maximum allowable amplitude of voltage ripple is 8.5% for a utilization of 98% [7].

On the other hand, at the output side of the inverter, the current going into the grid must be controlled to be sinusoidal and in phase with the grid voltage (unity power factor). There are certain regulations in this regard, and one important requirement

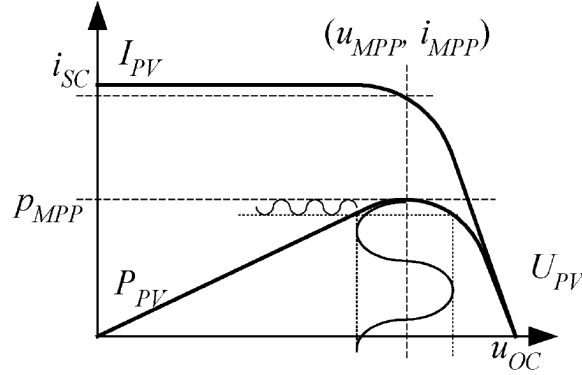


Figure 2.2: PV characteristics [7].

is that THD of the current must not exceed 5% [10]. Other supervisory controls, such as to disconnect the PV inverter from the grid in case of outage (anti-islanding), may also be required. It may also be required to supply reactive power (leading/lagging power factor).

For studying the basic control scheme, the inverter configurations studied so far can be categorized mainly as single-stage or two-stage. The central and string inverter configurations are usually single-stage while the multi-string and micro-inverter are two-stage configurations. In a single-stage configuration, both the input voltage and output current control must be performed by the full-bridge inverter stage. Usually a multi-loop strategy is applied as shown in Figure 2.3 [9], [11]. The outer loop is a voltage controller for the DC link capacitor. The reference for this controller comes from an MPPT block. This MPPT block is a separate controller which runs at a much lower frequency, that finds the required voltage across the PV so that maximum power is extracted. Algorithms such as Perturb and Observe (P&O), incremental conductance are widely used for it. The voltage controller output is a current reference for the grid side current, but is a DC quantity. This needs to be multiplied with the output of a phase-locked loop (PLL), locked with the grid voltage. The current controller then generates the PWM required to maintain this current.

For a two-stage configuration, the control scheme is as shown in Figure 2.4 [12].

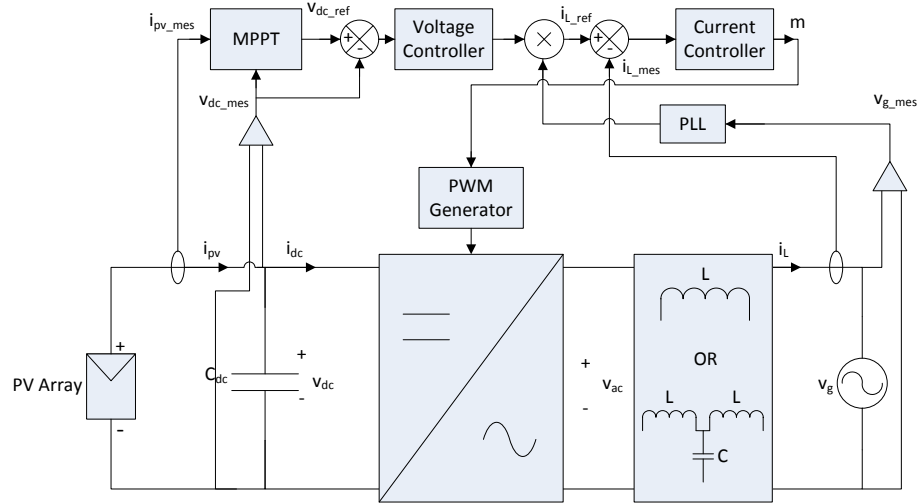


Figure 2.3: Single-stage grid-tie PV inverter control scheme.

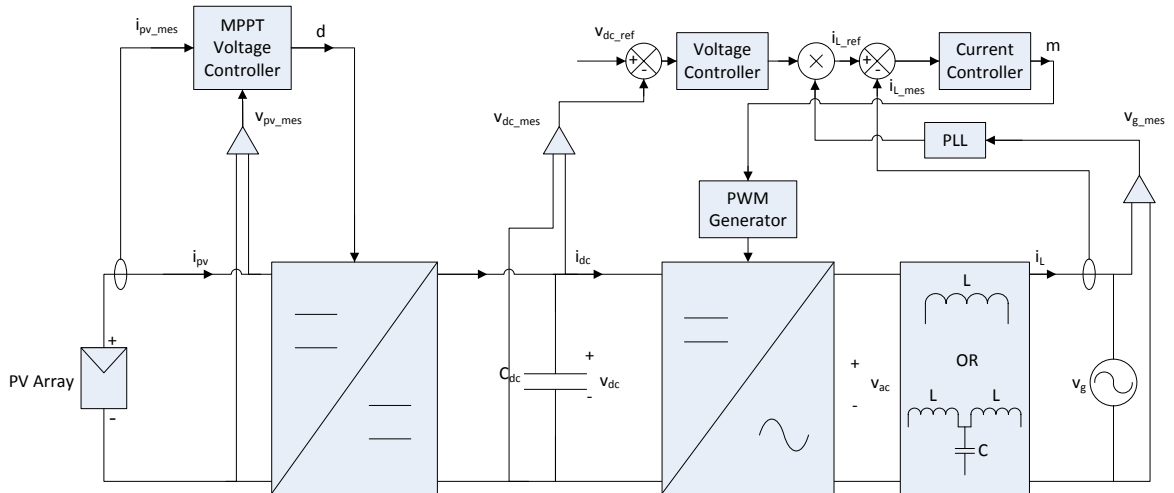


Figure 2.4: Two-stage grid-tie PV inverter control scheme.

Here, the DC-DC stage controls the PV side voltage based on the MPPT reference. The flexibility of the inverter stage to support the grid under varying PV power, increases due to the presence of this stage. This stage may be a boost, buck or buck-boost converter with a suitable topology. Usually it is a boost configuration, so that when the PV power goes down due to shading (cloud cover), a lower MPPT voltage (as required) is maintained at the input of this DC-DC stage and the output voltage can be much higher such that it can support the grid voltage. For a Micro-

inverter configuration, it is required to be a boost converter because very high step-up from panel voltage to grid voltage is required. The inverter controller is again a two-loop configuration, with the difference that the outer loop now controls the DC link capacitor voltage which is not the point of PV coupling [9].

2.3.1 Voltage Controller

The details of the control blocks considered in the above control structures will now be reviewed. The voltage controller block usually employs a proportional-integral (PI) controller to follow the reference capacitor voltage with zero steady-state error. But, the reference is a constant value, while the actual capacitor voltage has ripple. Thus, some methods are used to eliminate the ripple by filtering or by estimation. Low-pass or notch filters (tuned for 120 Hz) can be used to measure the voltage average value. Energy balance methods are used to estimate the capacitor stored energy over one switching cycle [13], one electrical cycle [14], [15] or half electrical cycle [12], and thus estimate the voltage ripple. This ripple can then be subtracted from the measured voltage to generate a constant current reference i.e. the current reference output of the controller is not affected by the voltage ripple. The advantage of this approach over filtering methods is that the controller frequency can be much higher than the grid frequency.

2.3.2 Current Controller

The current controller block is fed with a DC quantity as reference. But, the current to be controlled is AC. Thus, various methods are available to control the sinusoidal current and its phase with respect to grid voltage, such as instantaneous PI control, proportional-resonant (PR) stationary frame control, D-Q synchronous reference frame (SRF) PI control. All the methods require a phase-locked loop (PLL) based on the grid voltage. In instantaneous control, the output current is compared with the reference multiplied by the PLL output. Thus, the output of the PI controller

is a sinusoidal voltage reference or modulation index. The problem with this approach is that it is challenging to generate the AC reference to achieve zero steady-state error [16]. This is because the reference, for the output current to be in phase with grid, must account for the PI lag.

The PR controller also acts on the error of sinusoidal reference current (generated by multiplication of DC reference from previous voltage controller with required phase of PLL output) and measured AC current. The difference is in the transfer function of the controller. Unlike a PI, it can achieve infinite gain (theoretically) at the fundamental frequency, but practically very high gain can be achieved [18].

The D-Q transformation is usually used for the three-phase system where it is defined by the Park's transformation to convert the three phases (abc) to dq0. But, for a single phase system, the measured current first needs to be converted to the static frame ($\alpha\beta$), by creation of a second current (in quadrature with the real one). This can be achieved by various methods as described in [17], by delaying the real sinusoidal current by 90° , by obtaining capacitor current feedback or by using notch filters. The D-Q frame rotates with respect to $\alpha\beta$ frame as shown in Figure 2.5. The D-Q transformation matrix used, depends on the whether the current is aligned with sine or cosine function and whether the α and β are RMS or peak values. Here, we consider that they are RMS values and the D-Q components are peak values, thus we get a multiplying factor of $\sqrt{2}$. Thus, we get the following transformation matrices,

$$T = \sqrt{2} \begin{bmatrix} \cos(\theta) & \sin(\theta) \\ -\sin(\theta) & \cos(\theta) \end{bmatrix}, \quad T^{-1} = \frac{1}{\sqrt{2}} \begin{bmatrix} \cos(\theta) & -\sin(\theta) \\ \sin(\theta) & \cos(\theta) \end{bmatrix} \quad (2.1)$$

where,

$$\begin{bmatrix} \vec{v}_D \\ \vec{v}_Q \end{bmatrix} = T \begin{bmatrix} \vec{v}_\alpha \\ \vec{v}_\beta \end{bmatrix}, \quad \begin{bmatrix} \vec{v}_\alpha \\ \vec{v}_\beta \end{bmatrix} = T^{-1} \begin{bmatrix} \vec{v}_D \\ \vec{v}_Q \end{bmatrix} \quad (2.2)$$

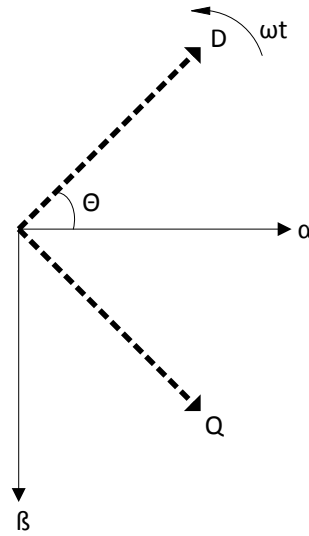
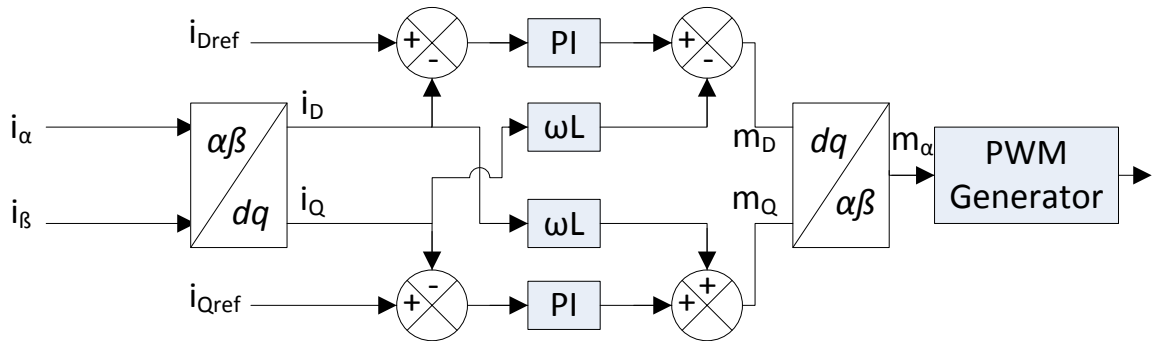
Figure 2.5: Relation between $\alpha\beta$ and D-Q frames.

Figure 2.6: D-Q controller.

The D-Q SRF controller structure is shown in Figure 2.6 [17]. The measured AC current is converted to its DC D and Q components. The reference obtained from the previous voltage control stage is usually compared with the D-component, while the Q-component reference depends on the required reactive power. Then two separate PI controllers are used to control these components. The output of these two PIs is some DC value as expected and needs to be converted back to sinusoidal reference using the inverse of D-Q transform. It can be seen that, it has additional decoupling terms (ωL) because the system model is such that they are coupled. This will be clear

in the next Chapter, where modeling is discussed.

Now, usually the output of any of the above current controllers goes to a PWM generator that generates the sinusoidal PWM (SPWM) for the full bridge inverter. Instead of controlling the average current (output of the filter stage after inverter) based on the sinusoidal reference (for example, by sine-triangle method), a peak current controller (PCC) can be used, in which the switching is directly controlled so that the current (output of the inverter, before filtering) follows the reference. PCC, though traditionally used for DC-DC converters, can also be used in inverters as mentioned in [19], with adequate slope-compensation near the peaks of the sine wave. There are other methods like hysteresis control, but it involves variable switching frequency.

2.4 Cascaded Multilevel Inverters

2.4.1 Topology and Operation

There has been a significant amount of research interest in the Multilevel Inverter topologies, especially the cascaded multilevel inverter or H-bridge (CHB). This is one of the commercial topologies of multilevel configuration and has the advantage of reliability owing to its modular structure [20]. In grid connected PV applications, each PV module can be connected to an H-bridge and they are series connected on the AC side to build up the voltage and then connected to the grid as shown in Figure 2.7. Each H-bridge is triggered with different modulation functions such that the sum of outputs (after filtering) is a sinusoid. The switching can either be at the fundamental frequency or a high frequency. Some modulation techniques like selective harmonic elimination (SHE), carrier based techniques like level-shifted and phase-shifted carriers, and space vector modulation (SVM) are used to generate the multilevel waveforms.

A common SHE technique, using fundamental switching frequency PWM is shown in Figure 2.8 (a). This technique has the disadvantage of unequal power distribution due to unequal conducting times [20]. The most common modulation technique used

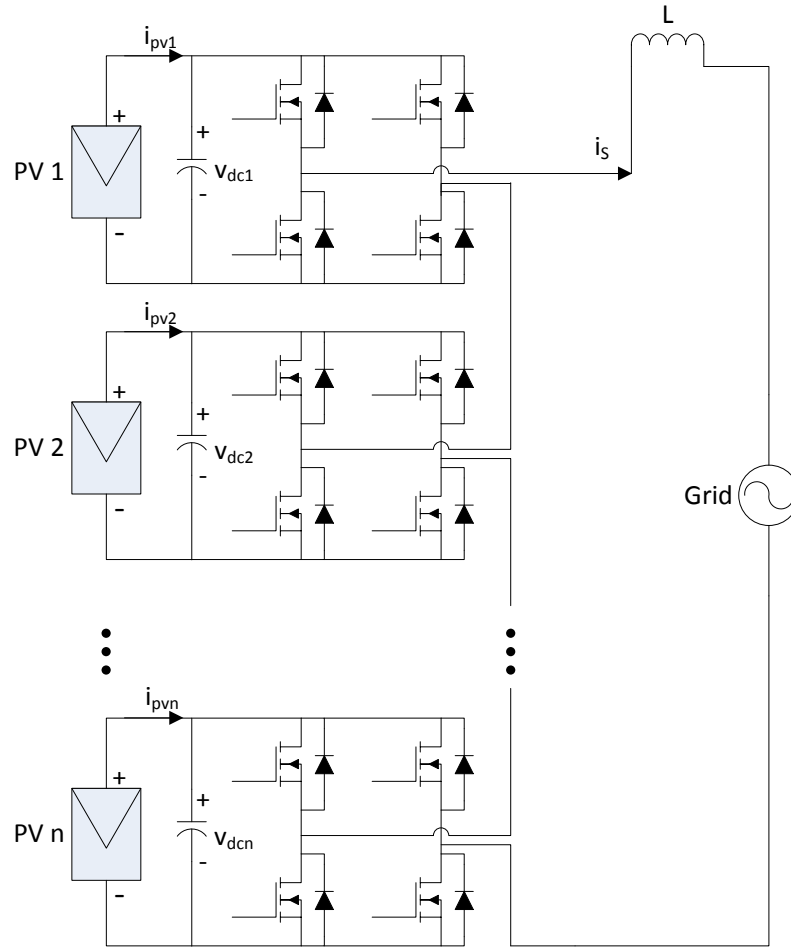


Figure 2.7: Cascaded H-bridge topology.

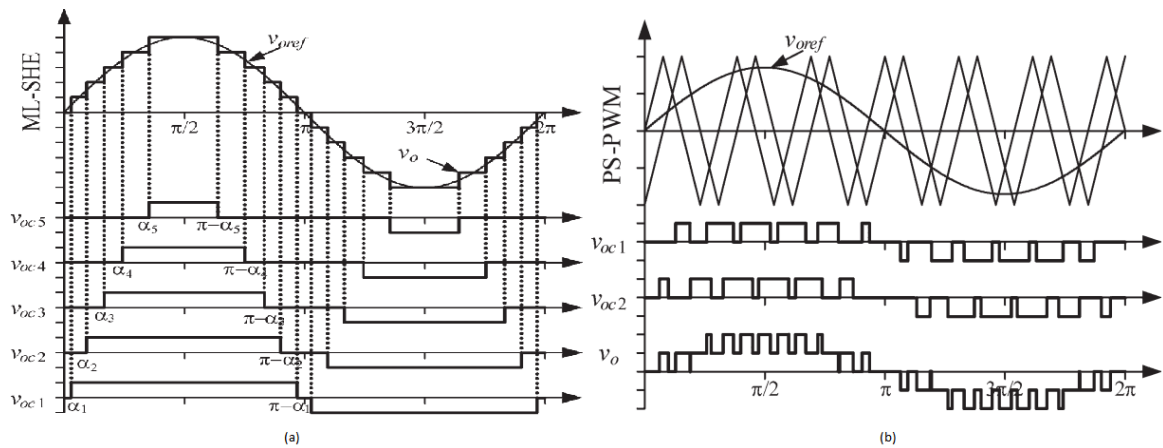


Figure 2.8: Multilevel modulation techniques: (a)SHE PWM (b)Phase-shifted PWM [20].

in CHB, is the phase-shifted carrier PWM which works as shown in Figure 2.8 (b). Here, phase shifted versions of a carrier signal are used to compare with the sinusoidal reference.

2.4.2 Control Scheme

The CHB configuration has the advantage of being a distributed PV architecture. But the control schemes usually employed are not completely distributed ones, they are either centralized or hybrid (centralized + distributed). A centralized control scheme is proposed by [21], as shown in figure 2.9. Here, the error of DC link voltage and its reference from individual MPPT stages is summed and total voltage control (PI) is performed on it. The output after multiplication with normalized PLL output gives the current reference. The error in string current is calculated and fed to the current controller (PR). The output of the current controller is the inductor voltage reference, which is added with the grid voltage measurement to get the total converter output voltage. Instead of directly using this output (normalized) as modulation index for each converter, an additional feedforward term, generated to control the DC link voltages of individual converters, is added to get individual modulation indices.

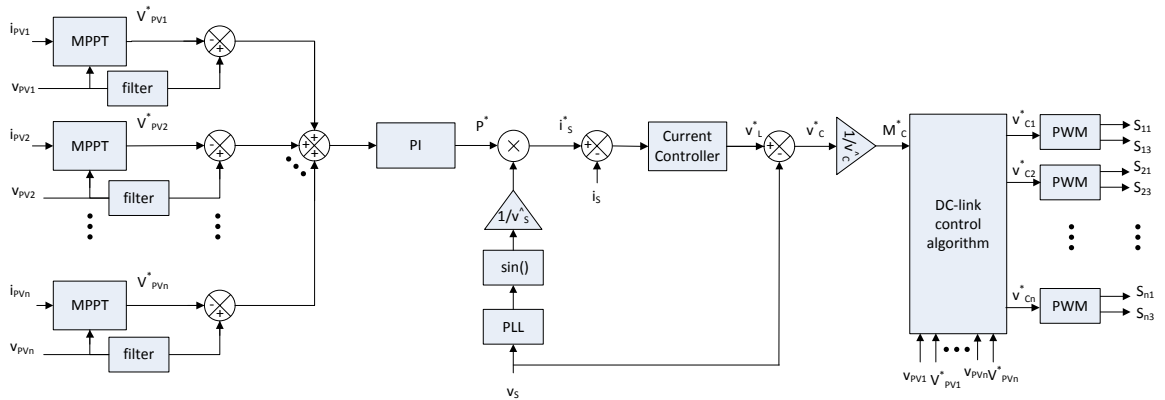


Figure 2.9: Centralized control scheme for CHB.

A typical hybrid control scheme proposed in [22] is shown in Figure 2.10. Individual, module-level MPPT is performed and the reference is used to control the

stage and the modulation function generation stage of the current controlling inverter, requires information from all other modules. At the same time, the modulation function generation of other inverters in cascade is only dependent on their own voltage controller. Hence, in this thesis, it is termed as a hybrid control scheme.

2.5 Inverter Molecule™

The IM configuration is similar to the CHB configuration studied in the previous section, with respect to the series connection of H-bridges. Many different embodiments of [6], provide different topologies (single-stage, two-stage, inverter with DC-DC converter parallel to DC bus called MFEC) for a common ideal of the configuration of AC stacked panel-level inverters. Of these, the single-stage inverter topology without the proprietary MFEC (which removes the 120 Hz DC bus ripple in single-phase inverters) is considered here¹, which is similar to the CHB configuration shown in Figure 2.7. The difference here is that each H-bridge output has a filter (LC) network and the connection to the grid is through an interface inductor. This difference is because the principle of operation is different - each inverter stage (with filtering) produces a sinusoidal voltage and current. Being a panel-level configuration, it takes the advantage of low voltage switches like MOSFETs, which can be switched at high frequencies to reduce the size of passive components required for filtering, in turn increasing power density. This also reduces cost in terms of the hardware. The BOS costs are much lower compared to central inverters as this configuration is panel-level like Micro-inverters. Also, the efficiency is higher compared to Micro-inverters as there is just one stage of conversion. The advantage of this configuration over a multilevel CHB is that the centralized control, required by CHB for the phase-shifted carrier for PWM generation of individual inverters, is not required for IM. This configuration however, requires a grid synchronized (PLL) signal for the reference generation

¹Throughout the thesis, this representation is used for the IM configuration for simplicity purposes, thus, not taking advantage of all the features of the IM architecture. However, the author does not claim that it is the only representation possible or that such advantages do not exist.

(modulation index) for each string member, which requires low bandwidth communication. According to an embodiment of [6], this function, along with other functions like string protection and anti-islanding, can be performed by a ‘Termination Box’ or ‘Load Center’ which interfaces the string to grid.

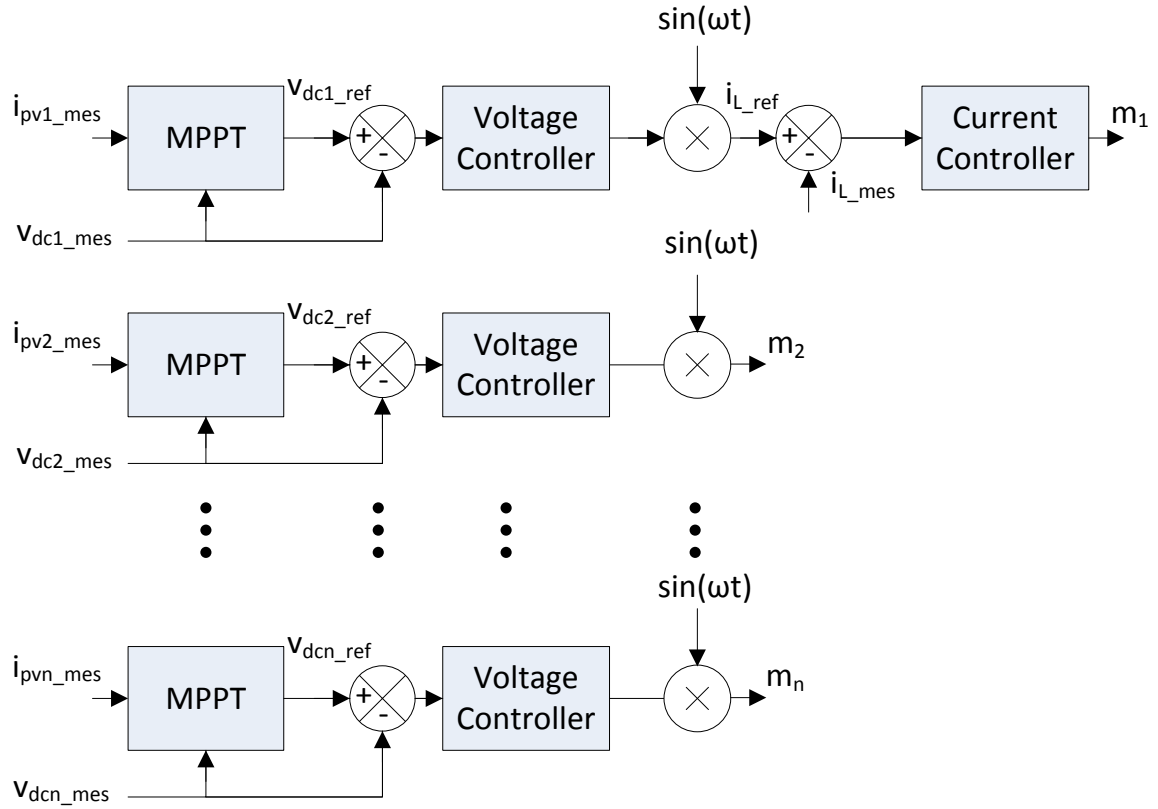


Figure 2.11: Distributed control scheme for IM.

The very fact that it is a series connected string of inverters, can be used to realize a truly distributed control scheme. Such a control scheme, based on an embodiment of [6], is shown in Figure 2.11. The string members do not require voltage or current information from other SMs. The inverter control depends only on locally measured voltage and current while the required information of other members is inherently carried through the AC side. Here, each SM controls its DC link voltage to extract maximum power. One of the SMs can be assigned the task of controlling the string current. This SM will be referred to as current administrator (CA). The CA controls

the string current by controlling its own power. If there is loss of power on any SM, resulting in the loss of string voltage, it will be translated to the DC side on account of power balance because the grid holds the string side voltage. This in turn will reduce the current in order to bring back the DC link that has gone up in voltage.

2.6 Conclusion

This chapter reviewed various grid-tie PV inverter configurations and their control schemes along with the advantages and disadvantages. The most promising configuration is the IM. Along with reducing the power electronics complexity, increasing efficiency and reducing costs, this configuration also provides the opportunity to realize a distributed control scheme. This thesis will thus make an attempt to design and develop the distributed control scheme using modern control theory approach and prove its feasibility.

CHAPTER 3: MODELING, ANALYSIS AND CONTROLLER DESIGN

3.1 Introduction

The main objective of this chapter is to derive the model of the Inverter Molecule™(IM) and by analyzing the model, design a suitable controller. The first step is the modeling of a single phase PV inverter, discussed in Section 3.2. Following this, a model for IM is derived and analyzed in Section 3.3. Then, based on the principle of state feedback control, using the distributed control method discussed in previous chapter, Section 2.5, the controller for IM is designed in Section 3.4 and the closed form is derived. The designed controller is analyzed under different operating points. The chapter is concluded with comments on the feasibility in Section 3.5.

3.2 Single Phase PV Inverter Modeling

The single-stage single phase, full bridge inverter for grid-tie PV application was studied in the previous chapter, Section 2.3 along with its control scheme. This section will discuss its state space modeling, based on the representation of Figure 3.1. In our modeling, we neglect the high frequency filter capacitor on the AC side. Also, as shown in Figure 3.1, the PV source is emulated as a DC voltage source in series with a resistor. Though the resistor has linear I-V characteristics, unlike PV, it is sufficient for our model because the concept of fixed input power based on controlling the DC capacitor voltage, the important characteristic of interest, is preserved.

Applying KVL to the output side of the inverter, we get,

$$v_{ac} - v_g = L \frac{di_L}{dt} \quad (3.1)$$

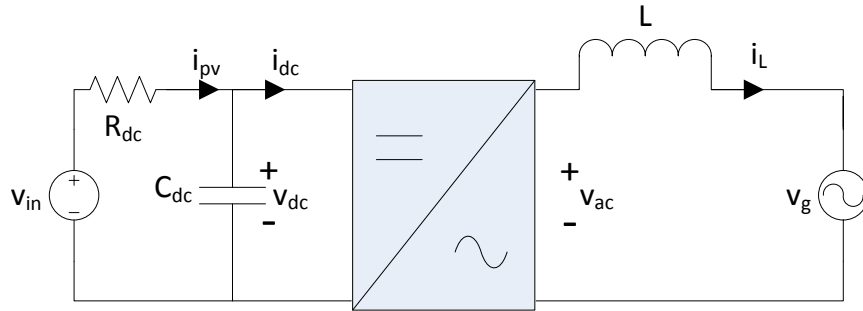


Figure 3.1: Single phase inverter.

Applying KCL to the DC capacitor, we get,

$$i_{pv} - i_{dc} = C_{dc} \frac{dv_{dc}}{dt} \quad (3.2)$$

The averaged switching function or the modulation index (m) of the inverter can be used to write, $v_{ac} = mv_{dc}$ and $i_{dc} = mi_L$ (based on power balance). Thus, also writing i_{pv} in terms of V_{in} , equations 3.1 and 3.2 become,

$$mv_{dc} - v_g = L \frac{di_L}{dt} \quad (3.3)$$

$$\frac{V_{in} - v_{dc}}{R_{dc}} - mi_L = C_{dc} \frac{dv_{dc}}{dt} \quad (3.4)$$

In order to analyze the time varying quantities, we convert them to synchronous rotating frame (SRF) using DQ transformation, discussed in the previous chapter, Sub-Section 2.3.2. Accordingly, the time-varying parameters must be converted to α and β phases. The actual parameters contribute to the α phase and their 90° phase shifted versions contribute to the imaginary or β phase. Equations 3.3 and 3.4 become,

$$\begin{aligned} m_\alpha v_{dc} - v_{g\alpha} &= L \frac{di_{L\alpha}}{dt} \\ m_\beta v_{dc} - v_{g\beta} &= L \frac{di_{L\beta}}{dt} \end{aligned} \quad (3.5)$$

$$\frac{V_{in} - v_{dc}}{R_{dc}} - m_{\alpha}i_{L\alpha} - m_{\beta}i_{L\beta} = C_{dc} \frac{dv_{dc}}{dt} \quad (3.6)$$

Combining α and β in equations (3.5) and (3.6),

$$\begin{bmatrix} m_{\alpha} \\ m_{\beta} \end{bmatrix} v_{dc} - \begin{bmatrix} v_{g\alpha} \\ v_{g\beta} \end{bmatrix} = L \frac{d}{dt} \begin{bmatrix} i_{L\alpha} \\ i_{L\beta} \end{bmatrix} \quad (3.7)$$

$$\frac{V_{in} - v_{dc}}{R_{dc}} - \begin{bmatrix} m_{\alpha} & m_{\beta} \end{bmatrix} \begin{bmatrix} i_{L\alpha} \\ i_{L\beta} \end{bmatrix} = C_{dc} \frac{dv_{dc}}{dt} \quad (3.8)$$

The transformation matrix (T) to convert from $\alpha\beta$ to D-Q, and its inverse are given in equation 2.1. Thus, converting the stationary frame terms in (3.7), to SRF using inverse of transformation matrix T^{-1} ,

$$T^{-1} \begin{bmatrix} m_D \\ m_Q \end{bmatrix} v_{dc} - T^{-1} \begin{bmatrix} v_{gD} \\ v_{gQ} \end{bmatrix} = L \frac{d}{dt} T^{-1} \begin{bmatrix} i_{LD} \\ i_{LQ} \end{bmatrix} \quad (3.9)$$

Multiplying (3.9) by transformation matrix T and simplifying,

$$\begin{bmatrix} m_D \\ m_Q \end{bmatrix} v_{dc} - \begin{bmatrix} v_{gD} \\ v_{gQ} \end{bmatrix} = L \begin{bmatrix} \dot{i}_{LD} - \omega i_{LQ} \\ \dot{i}_{LQ} + \omega i_{LD} \end{bmatrix} \quad (3.10)$$

Transforming equation (3.8) to synchronous frame using inverse of transformation matrix T^{-1} ,

$$\frac{V_{in} - v_{dc}}{R_{dc}} - \left(T^{-1} \begin{bmatrix} m_D \\ m_Q \end{bmatrix} \right)^T T^{-1} \begin{bmatrix} i_{LD} \\ i_{LQ} \end{bmatrix} = C_{dc} \frac{dv_{dc}}{dt} \quad (3.11)$$

Simplifying (3.11),

$$\frac{V_{in} - v_{dc}}{R_{dc}} - \frac{1}{2} \begin{bmatrix} m_D & m_Q \end{bmatrix} \begin{bmatrix} i_{LD} \\ i_{LQ} \end{bmatrix} = C_{dc} \dot{v}_{dc} \quad (3.12)$$

Now, equations(3.10) and (3.12), have non-linear terms. Thus, after adding perturbation and linearizing,

$$\begin{bmatrix} M_D \\ M_Q \end{bmatrix} \hat{v}_{dc} + \begin{bmatrix} \hat{m}_D \\ \hat{m}_Q \end{bmatrix} V_{dc} - \begin{bmatrix} v_{gD} \\ v_{gQ} \end{bmatrix} = L \begin{bmatrix} \dot{i}_{LD} - \omega \hat{i}_{LQ} \\ \dot{i}_{LQ} + \omega \hat{i}_{LD} \end{bmatrix} \quad (3.13)$$

$$\frac{V_{in} - \hat{v}_{dc}}{R_{dc}} - \frac{1}{2} \begin{bmatrix} \hat{m}_D & \hat{m}_Q \end{bmatrix} \begin{bmatrix} I_{LD} \\ I_{LQ} \end{bmatrix} - \frac{1}{2} \begin{bmatrix} M_D & M_Q \end{bmatrix} \begin{bmatrix} \hat{i}_{LD} \\ \hat{i}_{LQ} \end{bmatrix} = C_{dc} \dot{\hat{v}}_{dc} \quad (3.14)$$

In order to write the state space equations in standard form, the state variables, inputs and outputs must be specified. The inductor current D and Q components and the capacitor voltage will be the state variables. In PV applications the voltage at the point of PV coupling, in this case is the DC capacitor voltage, needs to be controlled in order to extract maximum power. Thus, \hat{v}_{dc} is an output variable. Also, the \hat{i}_{LQ} is also an output variable as it needs to be controlled. On the other hand, since the D-component of the output current is dependent on the input power and its value is not necessarily explicitly specified, it is not considered as an output. The modulation indices of the inverter and the grid voltage D-component, because Q-component is zero in a synchronized system, are considered inputs. Thus, system is summarized as below,

$$X = \begin{bmatrix} \hat{i}_{LD} \\ \hat{i}_{LQ} \\ \hat{v}_{dc} \end{bmatrix}, U = \begin{bmatrix} \hat{m}_D \\ \hat{m}_Q \\ v_{gD} \end{bmatrix}, Y = \begin{bmatrix} \hat{i}_{LQ} \\ \hat{v}_{dc} \end{bmatrix}$$

Considering the standard state space equations as,

$$\dot{X} = AX + BU$$

$$Y = CX + DU$$

We get the A , B , C , D matrices from (3.13) and (3.14) as follows,

$$A = \begin{bmatrix} 0 & \omega & \frac{M_D}{L} \\ -\omega & 0 & \frac{M_Q}{L} \\ \frac{-M_D}{2C_{dc}} & \frac{-M_Q}{2C_{dc}} & \frac{-1}{R_{dc}C_{dc}} \end{bmatrix} \quad (3.15)$$

$$B = \begin{bmatrix} \frac{V_{dc}}{L} & 0 & \frac{-1}{L} \\ 0 & \frac{V_{dc}}{L} & 0 \\ \frac{-I_{LD}}{2C_{dc}} & \frac{-I_{LQ}}{2C_{dc}} & 0 \end{bmatrix} \quad (3.16)$$

$$C = \begin{bmatrix} 0 & 1 & 0 \\ 0 & 0 & 1 \end{bmatrix}, \quad D = \begin{bmatrix} 0 & 0 & 0 \\ 0 & 0 & 0 \end{bmatrix} \quad (3.17)$$

3.3 Modeling and Analysis of IM

3.3.1 Modeling

The approach for deriving the model of IM will be similar to the previously derived single phase inverter model. The IM has been discussed in the previous chapter, Section 2.5. Figure 3.2 shows the representation of the IM for a string of two inverters. As considered in previous section, the output side has just one inductor (equivalent of filter inductors of both inverters and the grid connection inductor in series), the filter capacitors are ignored. Here, just two string members (SM) are considered as a minimal system, since it is enough to prove the concept.

Similar to equations (3.5) and (3.6) in the previous section, the differential equations for IM can be written from Figure 3.2 as,

$$\begin{aligned} m_{1\alpha}v_{dc1} + m_{2\alpha}v_{dc2} - v_{g\alpha} &= L \frac{di_{l\alpha}}{dt} \\ m_{1\beta}v_{dc1} + m_{2\beta}v_{dc2} - v_{g\beta} &= L \frac{di_{l\beta}}{dt} \end{aligned} \quad (3.18)$$

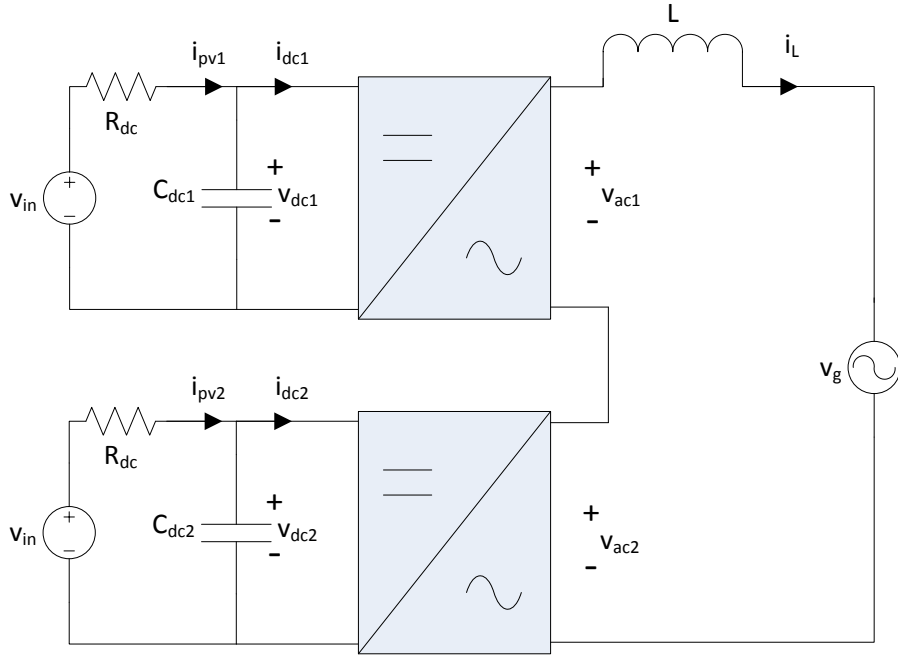


Figure 3.2: IM model.

$$\begin{aligned} \frac{V_{in} - v_{dc1}}{R_{dc}} - m_{1\alpha}i_{L\alpha} - m_{1\beta}i_{L\beta} &= C_{dc} \frac{dv_{dc1}}{dt} \\ \frac{V_{in} - v_{dc2}}{R_{dc}} - m_{2\alpha}i_{L\alpha} - m_{2\beta}i_{L\beta} &= C_{dc} \frac{dv_{dc2}}{dt} \end{aligned} \quad (3.19)$$

Combining α and β in equations (3.18) and (3.19),

$$v_{dc1} \begin{bmatrix} m_{1\alpha} \\ m_{1\beta} \end{bmatrix} + v_{dc2} \begin{bmatrix} m_{2\alpha} \\ m_{2\beta} \end{bmatrix} - \begin{bmatrix} v_{g\alpha} \\ v_{g\beta} \end{bmatrix} = L \begin{bmatrix} \dot{i}_{L\alpha} \\ \dot{i}_{L\beta} \end{bmatrix} \quad (3.20)$$

$$\frac{V_{in}}{R_{dc}} \begin{bmatrix} 1 \\ 1 \end{bmatrix} - \frac{1}{R_{dc}} \begin{bmatrix} v_{dc1} \\ v_{dc2} \end{bmatrix} - \begin{bmatrix} m_{1\alpha} & m_{1\beta} \\ m_{2\alpha} & m_{2\beta} \end{bmatrix} \begin{bmatrix} i_{L\alpha} \\ i_{L\beta} \end{bmatrix} = C_{dc} \begin{bmatrix} \dot{v}_{dc1} \\ \dot{v}_{dc2} \end{bmatrix} \quad (3.21)$$

Now, using the inverse of D-Q transformation matrix T^{-1} , equations (3.20) and (3.21) become,

$$\begin{bmatrix} m_{1D} \\ m_{1Q} \end{bmatrix} v_{dc1} + \begin{bmatrix} m_{2D} \\ m_{2Q} \end{bmatrix} v_{dc2} - \begin{bmatrix} v_{gD} \\ v_{gQ} \end{bmatrix} = L \begin{bmatrix} \dot{i}_{iD} - \omega i_{iQ} \\ \dot{i}_{iQ} + \omega i_{iD} \end{bmatrix} \quad (3.22)$$

$$\frac{V_{in}}{R_{dc}} \begin{bmatrix} 1 \\ 1 \end{bmatrix} - \frac{1}{R_{dc}} \begin{bmatrix} v_{dc1} \\ v_{dc2} \end{bmatrix} - \frac{1}{2} \begin{bmatrix} m_{1D} & m_{1Q} \\ m_{2D} & m_{2Q} \end{bmatrix} \begin{bmatrix} i_{LD} \\ i_{LQ} \end{bmatrix} = C_{dc} \begin{bmatrix} v_{dc1} \\ v_{dc2} \end{bmatrix} \quad (3.23)$$

After adding perturbation and linearizing the equations,

$$\begin{bmatrix} M_{1D} \\ M_{1Q} \end{bmatrix} v_{\hat{dc}1} + \begin{bmatrix} \hat{m}_{1D} \\ \hat{m}_{1Q} \end{bmatrix} V_{dc1} + \begin{bmatrix} M_{2D} \\ M_{2Q} \end{bmatrix} v_{\hat{dc}2} + \begin{bmatrix} \hat{m}_{2D} \\ \hat{m}_{2Q} \end{bmatrix} V_{dc2} - \begin{bmatrix} v_{gD} \\ v_{gQ} \end{bmatrix} \quad (3.24) \\ = L \begin{bmatrix} \dot{i}_{LD} - \omega \hat{i}_{LQ} \\ \dot{i}_{LQ} + \omega \hat{i}_{LD} \end{bmatrix}$$

$$\frac{V_{in}}{R_{dc}} \begin{bmatrix} 1 \\ 1 \end{bmatrix} - \frac{1}{R_{dc}} \begin{bmatrix} v_{\hat{dc}1} \\ v_{\hat{dc}2} \end{bmatrix} - \frac{1}{2} \begin{bmatrix} \hat{m}_{1D} & \hat{m}_{1Q} \\ \hat{m}_{2D} & \hat{m}_{2Q} \end{bmatrix} \begin{bmatrix} I_{LD} \\ I_{LQ} \end{bmatrix} - \frac{1}{2} \begin{bmatrix} M_{1D} & M_{1Q} \\ M_{2D} & M_{2Q} \end{bmatrix} \begin{bmatrix} \hat{i}_{LD} \\ \hat{i}_{LQ} \end{bmatrix} \quad (3.25) \\ = C_{dc} \begin{bmatrix} \dot{v}_{dc1} \\ \dot{v}_{dc2} \end{bmatrix}$$

Now, in order to derive the small-signal state space model, we consider the state variables, input and output variables similar to previous section, as follows,

$$X = \begin{bmatrix} \hat{i}_{LD} \\ \hat{i}_{LQ} \\ v_{\hat{dc}1} \\ v_{\hat{dc}2} \end{bmatrix}, U = \begin{bmatrix} \hat{m}_{1D} \\ \hat{m}_{1Q} \\ \hat{m}_{2D} \\ \hat{m}_{2Q} \\ v_{gD} \end{bmatrix}, Y = \begin{bmatrix} \hat{i}_{LQ} \\ v_{dc1} \\ v_{dc2} \end{bmatrix}$$

Thus, based on the equations (3.24) and (3.25), we get the A , B , C , D matrices as

follows,

$$A = \begin{bmatrix} 0 & \omega & \frac{M_{1D}}{L} & \frac{M_{2D}}{L} \\ -\omega & 0 & \frac{M_{1Q}}{L} & \frac{M_{2Q}}{L} \\ \frac{-M_{1D}}{2C_{dc}} & \frac{-M_{1Q}}{2C_{dc}} & \frac{-1}{R_{dc}C_{dc}} & 0 \\ \frac{-M_{2D}}{2C_{dc}} & \frac{-M_{2Q}}{2C_{dc}} & 0 & \frac{-1}{R_{dc}C_{dc}} \end{bmatrix} \quad (3.26)$$

$$B = \begin{bmatrix} \frac{V_{dc1}}{L} & 0 & \frac{V_{dc2}}{L} & 0 & \frac{-1}{L} \\ 0 & \frac{V_{dc1}}{L} & 0 & \frac{V_{dc2}}{L} & 0 \\ \frac{-I_{LD}}{2C_{dc}} & \frac{-I_{LQ}}{2C_{dc}} & 0 & 0 & 0 \\ 0 & 0 & \frac{-I_{LD}}{2C_{dc}} & \frac{-I_{LQ}}{2C_{dc}} & 0 \end{bmatrix} \quad (3.27)$$

$$C = \begin{bmatrix} 0 & 1 & 0 & 0 \\ 0 & 0 & 1 & 0 \\ 0 & 0 & 0 & 1 \end{bmatrix}, \quad D = \begin{bmatrix} 0 & 0 & 0 & 0 & 0 \\ 0 & 0 & 0 & 0 & 0 \\ 0 & 0 & 0 & 0 & 0 \end{bmatrix} \quad (3.28)$$

3.3.2 Analysis

Now, after deriving the state space for IM, finding the values of these matrices for a steady state operating point is desirable. In the system described in Figure 3.2, V_{in} is assumed to be the open circuit voltage for a PV panel. From the V_{OC} specification of a 285 W PV panel, $V_{in} = 39.7$ V [25]. Now, in order to emulate a PV at MPPT, in steady state $V_{dc1} = 31.3$ and $V_{dc2} = 31.3$, based on the V_{mpp} specification of a PV panel [25]. But at the same time the value of R_{dc} must also be set based on the I_{mpp} of the panel as $R_{dc} = (V_{in} - V_{dc1})/I_{mpp} = 0.9231$. The value of C_{dc} , the electrolytic capacitors, is assumed to be 10 mF.

Two string member inverters with their DC voltages as above can be used to support a grid voltage of 50 V (stepped down), because it is essential that the required modulation index should not be 1 (100%), so that the string of inverters can support the grid even at less than maximum power. The Q-component of the grid voltage is zero, thus the peak value of grid voltage, $V_{gD} = 50$ V, $V_{gQ} = 0$ V. Now, assuming

no losses, the peak of output current, $I_{LD} = 2P_{dc}/V_{gD} = 22.786$ A and $I_{LQ} = 0$ A for zero reactive power compensation. The inductor is assumed to be 75 μ H, as the switching frequency is 100 kHz.

In order to find the steady state values of the modulation indices of the two inverters, we use equations (3.22) and (3.23) to derive steady state equations, by adding perturbation and retaining the DC terms, as follows,

$$\begin{bmatrix} M_{1D} \\ M_{1Q} \end{bmatrix} V_{dc1} + \begin{bmatrix} M_{2D} \\ M_{2Q} \end{bmatrix} V_{dc2} - \begin{bmatrix} V_{gD} \\ V_{gQ} \end{bmatrix} + L \begin{bmatrix} \omega I_{LQ} \\ -\omega I_{LD} \end{bmatrix} = 0 \quad (3.29)$$

$$\frac{V_{in}}{R_{dc}} \begin{bmatrix} 1 \\ 1 \end{bmatrix} - \frac{1}{R_{dc}} \begin{bmatrix} V_{dc1} \\ V_{dc2} \end{bmatrix} - \begin{bmatrix} M_{1D} & M_{1Q} \\ M_{2D} & M_{2Q} \end{bmatrix} \begin{bmatrix} I_{LD} \\ I_{LQ} \end{bmatrix} = 0 \quad (3.30)$$

Substituting the values assumed above in the equations (3.29) and (3.30), we get the nominal symmetric modulation indices as,

$$M_{1D} = 0.7987, M_{1Q} = 0.0206, M_{2D} = 0.7987, M_{2Q} = 0$$

These nominal operating points can be summarized as in Table 3.1.

Based on the above values for a steady state operating point, we get the A and B matrices as follows,

$$A = \begin{bmatrix} 0 & 120\pi & 1.065 \times 10^4 & 1.065 \times 10^4 \\ -120\pi & 0 & 274.441 & 0 \\ -39.936 & -1.029 & -108.331 & 0 \\ -39.936 & 0 & 0 & -108.331 \end{bmatrix} \quad (3.31)$$

Table 3.1: Nominal operating points.

V_{in}	39.7 V
R_{dc}	0.9231 Ω
V_{dc1}, V_{dc2}	31.3 V
V_{gD}	50 V
V_{gQ}	0 V
I_{LD}	22.786 A
I_{LQ}	0 A
M_{1D}	0.7987
M_{1Q}	0.0206
M_{2D}	0.7987
M_{2Q}	0
L	75 μ H
C_{dc}	10 mF

$$B = \begin{bmatrix} 4.173 \times 10^5 & 0 & 4.173 \times 10^5 & 0 & -1.333 \times 10^4 \\ 0 & 4.173 \times 10^5 & 0 & 4.173 \times 10^5 & 0 \\ -1.139 \times 10^3 & 0 & 0 & 0 & 0 \\ 0 & 0 & -1.139 \times 10^3 & 0 & 0 \end{bmatrix} \quad (3.32)$$

The eigenvalues of the above obtained system matrix A can be found to analyze the stability of the system as follows,

$$eig_A = \begin{bmatrix} -46.4762 + 994.643 i \\ -46.4762 - 994.643 i \\ -16.969 \\ -107.08 \end{bmatrix} \quad (3.33)$$

The eigenvalues are found using MATLAB function 'eig()', which lists the eigenvalues in the order of the state variables. As observed, the eigenvalues have negative real parts, indicating that the system is stable. But, the values are not very big in magnitude, indicating that the poles of the system are close to the origin and might go

to the right half for other operating points. Also, it can be seen that the eigenvalues corresponding to i_{LD} and i_{LQ} have a large imaginary part indicating that there are oscillations and the system is not completely damped.

It is desirable to have a completely damped system and also push the poles further into the left half. It is also required that the system be decoupled to some extent, meaning that change in a state variable should not affect another state variable. Here, we know that a change in v_{dc1} should not affect v_{dc2} and vice versa, and it is true based on the A matrix obtained above. But also, i_{LD} and i_{LQ} must be decoupled, which is not the case as can be seen in the A matrix. Similarly, there is some degree of decoupling required between inputs and outputs in a MIMO system as we have, meaning that one output should not get affected by all inputs. For example, we know that a change in modulation index of one SM must not affect the input voltage or the power of another SM. It is thus required to have a closed loop control and add a feedback that changes these system properties as desirable.

3.4 Feedback Control Design for IM

3.4.1 Formulation

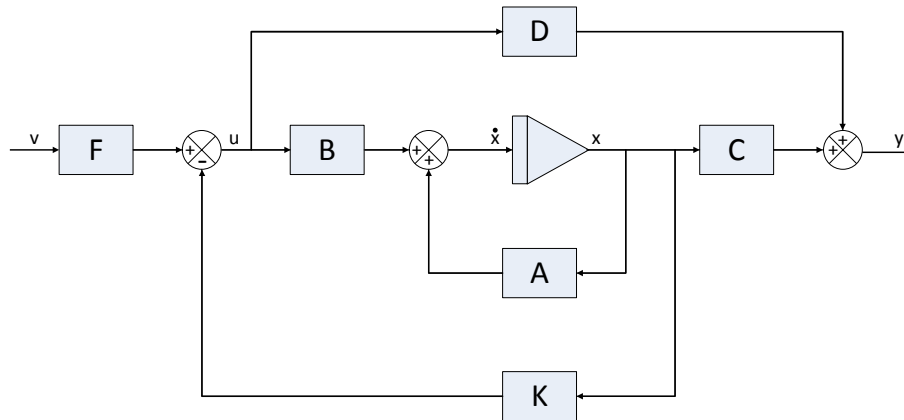


Figure 3.3: State variable feedback system.

In order to design the controller for IM, the principle of state variable feedback [26] will be applied. Figure 3.3 shows the block diagram of a general system with

state feedback. Here, v is the reference input, K is the feedback matrix and F is the input reference feedforward matrix. The way in which the feedback and feedforward matrices affect the system state space model can be seen by the equations that follow [26].

The input has now changed to,

$$u = Fv - Kx \quad (3.34)$$

Thus, the standard state equation $\dot{x} = Ax + Bu$ becomes,

$$\dot{x} = Ax + B(Fv - Kx) \quad (3.35)$$

$$\dot{x} = (A - BK)x + (BF)v \quad (3.36)$$

Thus, from equation (3.36), it can be seen that the system matrix and input matrix change to,

$$A_{CL} = A - BK, \quad B_{CL} = BF \quad (3.37)$$

Now for the model of IM, (3.34) can be re-written as,

$$\begin{bmatrix} \hat{m}_{1D} \\ \hat{m}_{1Q} \\ \hat{m}_{2D} \\ \hat{m}_{2Q} \\ \hat{v}_{gD} \end{bmatrix} = \begin{bmatrix} F_{11} & F_{12} & F_{13} \\ F_{21} & F_{22} & F_{23} \\ F_{31} & F_{32} & F_{33} \\ F_{41} & F_{42} & F_{43} \\ F_{51} & F_{52} & F_{53} \end{bmatrix} \begin{bmatrix} \hat{i}_{LQref} \\ v_{dc1ref} \\ v_{dc2ref} \end{bmatrix} - \begin{bmatrix} K_{11} & K_{12} & K_{13} & K_{14} \\ K_{21} & K_{22} & K_{23} & K_{24} \\ K_{31} & K_{32} & K_{33} & K_{34} \\ K_{41} & K_{42} & K_{43} & K_{44} \\ K_{51} & K_{52} & K_{53} & K_{54} \end{bmatrix} \begin{bmatrix} \hat{i}_{LD} \\ \hat{i}_{LQ} \\ v_{dc1} \\ v_{dc2} \end{bmatrix} \quad (3.38)$$

Ideally, a system should be completely decoupled, so that the system matrix A is diagonal. But for our system of IM, i_{LD} must depend upon v_{dc1} and v_{dc2} . i_{LD} and i_{LQ} should be decoupled from each other. But i_{LQ} should not depend on either DC voltages, because it is preferable that reactive power is not supplied by the DC

side. The v_{dc1} and v_{dc2} must be completely decoupled because it is not desirable that if one SM loses power, the maximum power extracting capability of other SM is compromised. Thus, the feedback matrix must be designed such that the closed loop system matrix A_{CL} looks like,

$$A_{CL} = \begin{bmatrix} A_{11} & 0 & A_{13} & A_{14} \\ 0 & A_{22} & 0 & 0 \\ 0 & 0 & A_{33} & 0 \\ 0 & 0 & 0 & A_{44} \end{bmatrix} \quad (3.39)$$

Now, the aim is to design a distributed control architecture with just one SM controlling the current (CA) while all others (including the CA) are controlling their input voltage to extract maximum power. By observing equation (3.38), the elements of the K matrix that violate the distributed control requirement must be eliminated. The input $m_{\hat{1}D}$, of SM1 which is the current controller, must only depend on $i_{\hat{L}D}$ and $v_{\hat{dc}1}$. But since the system matrix A has cross coupling term ω as seen in equation (3.31), this input should also feed back $i_{\hat{L}Q}$ in order to decouple it. Similarly for $m_{\hat{1}Q}$, $i_{\hat{L}D}$ and $v_{\hat{dc}1}$ must be fed back in order to decouple them. Now, $m_{\hat{2}D}$ should only depend on $v_{\hat{dc}2}$ because SM2 is not responsible for controlling current. Similarly, $m_{\hat{2}Q}$ must not have feedback of $i_{\hat{L}Q}$ and also $v_{\hat{dc}2}$. The input $v_{\hat{g}D}$ does not depend on any state variable. The feedback matrix, based on this method, must look like,

$$K = \begin{bmatrix} K_{11} & K_{12} & K_{13} & 0 \\ K_{21} & K_{22} & K_{23} & 0 \\ 0 & 0 & 0 & K_{34} \\ 0 & 0 & 0 & 0 \\ 0 & 0 & 0 & 0 \end{bmatrix} \quad (3.40)$$

The F matrix can be built with constraints similar to the ones considered for K

above. Firstly, consider the decoupling required in the input matrix of the closed loop system B_{CL} . This input matrix now relates the state variables to the reference inputs. The elements of the reference vector v from equation (3.38) are $i_{LQ\hat{ref}}$, $v_{dc1\hat{ref}}$, $v_{dc2\hat{ref}}$. The state variable i_{LD} will depend on both $v_{dc1\hat{ref}}$ and $v_{dc2\hat{ref}}$. But the other state variables will only depend on their respective references. Thus B_{CL} must look like,

$$B_{CL} = \begin{bmatrix} 0 & B_{12} & B_{13} \\ B_{21} & 0 & 0 \\ 0 & B_{32} & 0 \\ 0 & 0 & B_{43} \end{bmatrix} \quad (3.41)$$

Now, considering the distributed control method required and referring equation (3.38), we attempt to eliminate the elements of F matrix. The system input m_{1D} depends on $v_{dc1\hat{ref}}$ only, while the input m_{1Q} depends on $v_{dc2\hat{ref}}$. As we already know, v_{gD} is completely independent. The Q-components of the modulation of both SMs only depends on $i_{LQ\hat{ref}}$. Thus, the reference feedforward matrix looks like,

$$F = \begin{bmatrix} 0 & F_{12} & 0 \\ F_{21} & 0 & 0 \\ 0 & 0 & F_{33} \\ F_{41} & 0 & 0 \\ 0 & 0 & 0 \end{bmatrix} \quad (3.42)$$

3.4.2 Analytical Design

Considering the K , A and B from equations (3.40), (3.31) and (3.32) for nominal symmetric operating points (steady-state), we get the closed loop system matrix as,

$$A_{CL} = \begin{bmatrix} \frac{-V_{dc1}K_{11}}{L} & \omega - \frac{-V_{dc1}K_{12}}{L} & \frac{M_{1D}-V_{dc1}K_{13}}{L} & \frac{M_{2D}-V_{dc2}K_{34}}{L} \\ -\omega - \frac{-V_{dc1}K_{21}}{L} & \frac{-V_{dc1}K_{22}}{L} & \frac{M_{1Q}-V_{dc1}K_{23}}{L} & \frac{M_{2Q}}{L} \\ \frac{I_{LD}K_{11}-M_{1D}}{2C_{dc}} & \frac{I_{LD}K_{12}-M_{1Q}}{2C_{dc}} & \frac{I_{LD}K_{13}R_{dc}-2}{2C_{dc}R_{dc}} & 0 \\ \frac{-M_{2D}}{2C_{dc}} & \frac{-M_{2Q}}{2C_{dc}} & 0 & \frac{I_{LD}K_{34}R_{dc}-2}{2C_{dc}R_{dc}} \end{bmatrix} \quad (3.43)$$

Equating this above obtained matrix with the one from equation (3.39), the following values of the K matrix are found,

$$\begin{aligned} K_{11} &= \frac{M_{1D}}{I_{LD}} = 0.03506 \\ K_{12} &= \frac{\omega L}{V_{dc1}} = 0.000903 \\ K_{21} &= \frac{-\omega L}{V_{dc1}} = -0.000903 \\ K_{23} &= \frac{M_{1Q}}{V_{dc1}} = 0.000658 \end{aligned}$$

It is also found that the A_{CL} matrix has the term which makes v_{dc2} dependent on i_{LD} . This could be removed by adding the term K_{31} in the feedback matrix, but this does not conform with our distributed control architecture i.e. the SM which is not controlling current must not have current feedback.

For the other values of the feedback matrix, K_{13} , K_{22} , K_{34} there will be numerous possibilities. These possibilities can be found by checking for the eigenvalues of $A-BK$ for stability (negative real parts) and complete damping (zero imaginary parts). An additional condition based on the response time can be checked for, i.e. the eigenvalues corresponding to current should be much more negative than those corresponding to the two DC capacitor voltages. This is because, in a multi-loop control system, the

inner loop is much faster than the outer loop. Thus, eigenvalues for current can be selected to between $f_{sw}/2$ and $f_{sw}/10$, where f_{sw} is the switching frequency, and eigenvalues for v_{dc1} and v_{dc2} can be $1/5^{th}$ of that. An additional condition that, the eigenvalue for the DC voltage of current controller should be two times faster than other DC voltage, can be used. The implication of this is that the current controller SM also compensates for the voltage if an SM loses its power. This condition should be used, if the current controller is the most powerful SM [6]. Thus, by loop iterations in MATLAB to meet the above conditions of eigenvalues, many different combinations of values of K_{13}, K_{22}, K_{34} are found. Around 2000 combinations are found for iterating the values of these K elements in steps of 0.01. More can be found by decreasing the step size. The selected values of K and the eigenvalues of the closed loop system are,

$$K = \begin{bmatrix} 0.03506 & 0.000903 & -1 & 0 \\ -0.000903 & 0.09 & 0.000658 & 0 \\ 0 & 0 & 0 & -0.98 \\ 0 & 0 & 0 & 0 \\ 0 & 0 & 0 & 0 \end{bmatrix}, eig_{ACL} = \begin{bmatrix} -37.56 \times 10^3 \\ -13.21 \times 10^3 \\ -2.623 \times 10^3 \\ -1.248 \times 10^3 \end{bmatrix} \quad (3.44)$$

Now, by multiplying the F from equation (3.42) with the B matrix from equation (3.32) we do get the input matrix of equation (3.41). Thus, we cannot find the values of the remaining elements of the F matrix. So, we need to find the values of F based on the closed loop transfer function. Taking Laplace transform of equation (3.36),

$$sx(s) = (A - BK)x(s) + (BF)v(s) \quad (3.45)$$

$$x(s) = ((sI - (A - BK))^{-1})(BF)v(s) \quad (3.46)$$

Substituting this in $y(s) = Cx(s) + Dv(s)$,

$$y(s) = C((sI - (A - BK))^{-1})(BF)v(s) + 0 \quad (3.47)$$

Thus, we get the closed loop transfer function as,

$$G(s) = \frac{y(s)}{v(s)} = C((sI - (A - BK))^{-1})(BF) \quad (3.48)$$

Substituting A matrix from (3.31), B matrix from (3.32), K and F matrices from equations (3.44) and (3.42), in above equation and doing symbolic calculation in Mathcad for steady-state transfer function, we get,

$$G_{CL}(0) = \begin{bmatrix} 1.11F_{21} + 1.11F_{41} & 0 & 0 \\ 0 & -0.913F_{12} & 0 \\ 0 & -0.031F_{12} & -0.961F_{33} \end{bmatrix} \quad (3.49)$$

We know that the above obtained $G_{CL}(s)$ must be an identity matrix, so that the reference is tracked exactly and is not dependent on other references. Here, we can find F_{33} , but F_{21} and F_{41} can not be solved for without assuming either one. This shows that the Q-component of the current that contributes to reactive power, is shared by both SMs equally and only depends on the i_{LQref} . We assume 0.045 for both. Also, there is a compromise between making v_{dc1} track the reference and making v_{dc2} independent of v_{dc1} for finding F_{12} . If the latter is considered, than it makes v_{dc1} completely independent of its reference (by making the $G_{CL_{2,2}}$ zero), which is not acceptable. Thus, the reference tracking capability of v_{dc1} is given importance and we

get the following F matrix,

$$F = \begin{bmatrix} 0 & -1.095 & 0 \\ 0.045 & 0 & 0 \\ 0 & 0 & -1.04 \\ 0.045 & 0 & 0 \\ 0 & 0 & 0 \end{bmatrix} \quad (3.50)$$

The closed form looks like,

$$G_{CL}(0) = \begin{bmatrix} 1 & 0 & 0 \\ 0 & 1 & 0 \\ 0 & 33 \times 10^{-3} & 1 \end{bmatrix} \quad (3.51)$$

The penalty paid for not making the closed form completely equivalent to identity matrix, which was possible if current was fed back to the second SM which is not the current controller, should now be studied.

The step response of the closed loop system is shown in Figure 3.4. It can be seen from all the step responses that the response times are as expected based on the feedback gains selected. The response of a state variable to other references has some disturbance, but it is very minor, and settles at around zero. Only when there is a step change in v_{dc1ref} , the v_{dc2} changes slightly, but also settles close to zero very quickly.

3.4.3 Asymmetric Operation Analysis

After designing the controller, it is now desirable to analyze the impact of changes in the steady state operation. Due to cloud presence during daytime, the output of some of the PV panels may get affected, resulting in lower power to the inverter input of some string members. This, will in turn reduce the string output power, but it

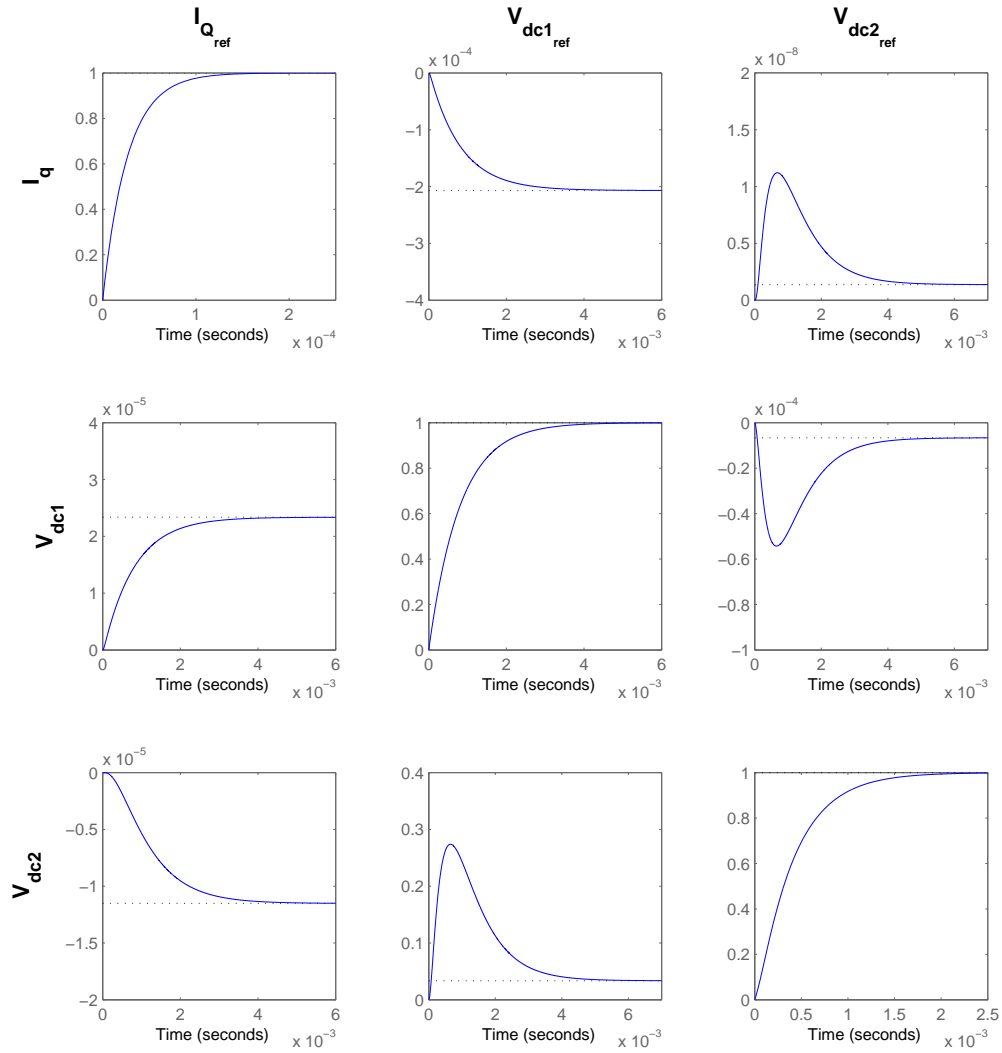


Figure 3.4: Step response of closed loop system.

must not affect the MPP of the other SMs.

Assume that, in the two SM system considered so far, SM2 loses power. This effect can be emulated by changing the V_{in} of that SM. But, the V_{dc2} also needs to change in order to extract maximum power at this reduced power level. Let the new values be, $V_{in2} = 36$, $V_{dc2} = 30$. Keeping the value of R_{dc} same, we get the output current as

$I_{LD} = 19.193$. Substituting these values in equations (3.24) and (3.25),

$$M_{1D} = 0.948$$

$$M_{1Q} = 0.021$$

$$M_{2D} = 0.677$$

$$M_{2Q} = 0$$

The values for asymmetric operation are summarized in Table 3.2

Table 3.2: Asymmetric operating points.

V_{in1}	39.7 V
V_{in2}	36 V
R_{dc}	0.9231 Ω
V_{dc1}	31.3 V
V_{dc2}	30 V
V_{gD}	50 V
V_{gQ}	0 V
I_{LD}	19.19 A
I_{LQ}	0 A
M_{1D}	0.948
M_{1Q}	0.021
M_{2D}	0.677
M_{2Q}	0
L	75 μH
C_{dc}	10 mF

Substituting these values in equations (3.26) and (3.27),

$$A = \begin{bmatrix} 0 & 120\pi & 1.264 \times 10^4 & 9.031 \times 10^3 \\ -120\pi & 0 & 274.441 & 0 \\ -47.413 & -1.029 & -108.331 & 0 \\ -33.866 & 0 & 0 & -108.331 \end{bmatrix} \quad (3.52)$$

$$B = \begin{bmatrix} 4.173 \times 10^5 & 0 & 4 \times 10^5 & 0 & -1.333 \times 10^4 \\ 0 & 4.173 \times 10^5 & 0 & 4 \times 10^5 & 0 \\ -959.636 & 0 & 0 & 0 & 0 \\ 0 & 0 & -959.636 & 0 & 0 \end{bmatrix} \quad (3.53)$$

Based on these new values for the system and input matrix and considering the same gains for feedback and feedforward, we get the closed form as follows,

$$G_{CL}(0) = \begin{bmatrix} 1 & 0 & 0 \\ -1.264 \times 10^{-4} & 0.997 & 13 \times 10^{-3} \\ 6.37 \times 10^{-5} & 33 \times 10^{-3} & 0.985 \end{bmatrix} \quad (3.54)$$

As it can be seen, it has changed from the closed loop transfer function obtained for nominal values. The reference tracking of the two DC voltages has been affected negatively by a small margin.

The step response for the new asymmetric system with same K and F is show in Figure 3.5. As it can be observed, the step response is very similar to the one obtained for nominal operating points in Figure 3.4. There is a very small error in the reference tracking on all the state variables. The response of a state variable to others is very small and quickly settles close to zero except for the effect of the DC voltages on each other. In addition to the effect of v_{dc1ref} on v_{dc2} , as seen in previous step response, there is also a similar effect of v_{dc2ref} on v_{dc1} . But both settle close to zero very quickly.

3.5 Conclusion

This chapter laid the mathematical foundation for the Inverter Molecule™ by deriving a linearized state space model. Then, a distributed control scheme was designed and analyzed using modern control theory approach. It was also analyzed for operating points other than what is was designed for. The control scheme provided the

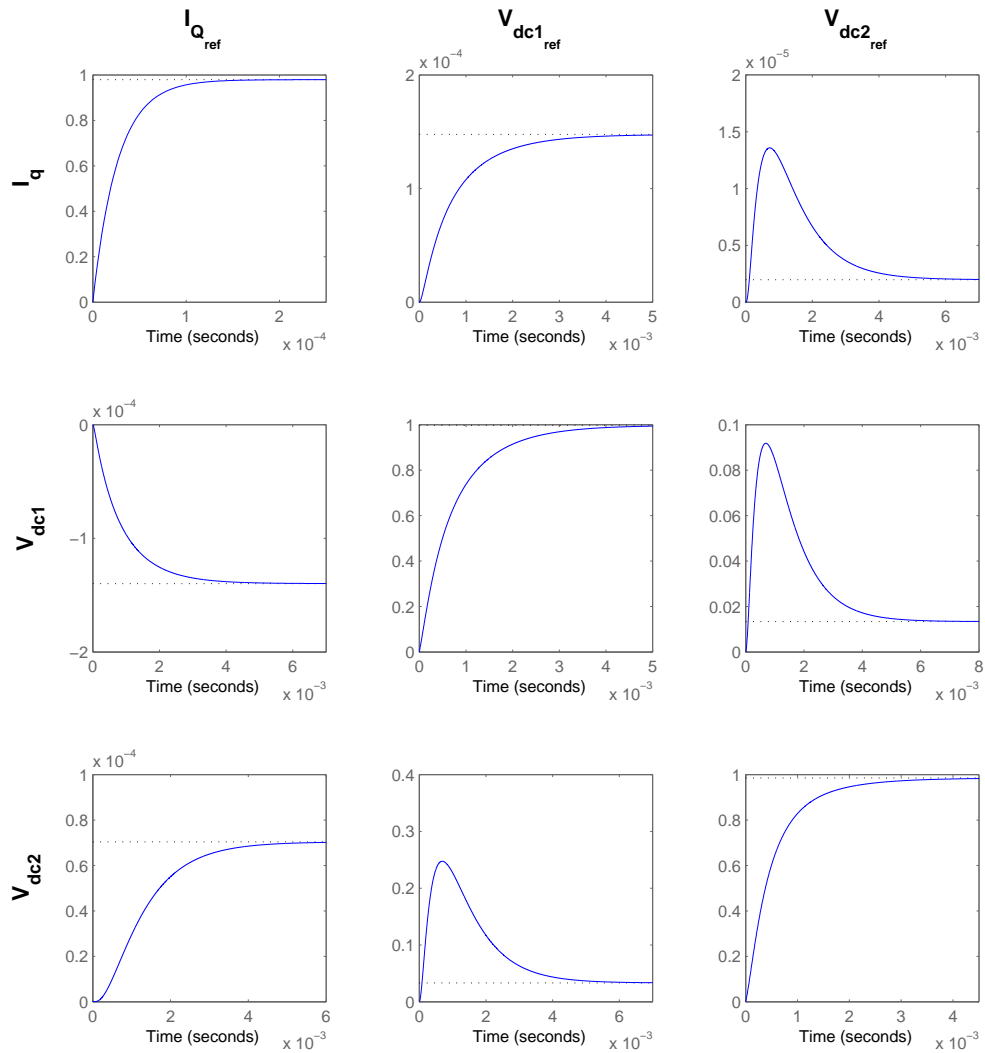


Figure 3.5: Step response of closed loop system with asymmetric operating points.

essential characteristics of stability, fast response, reference tracking and the required degree of decoupling. These characteristics also held true for an asymmetrical operating point, keeping the gains constant, with acceptable margin of error. Thus, it proves the feasibility of this distributed control scheme for IM. The visualization of the IM architecture with the distributed control thus designed can be seen in Figure 3.6.

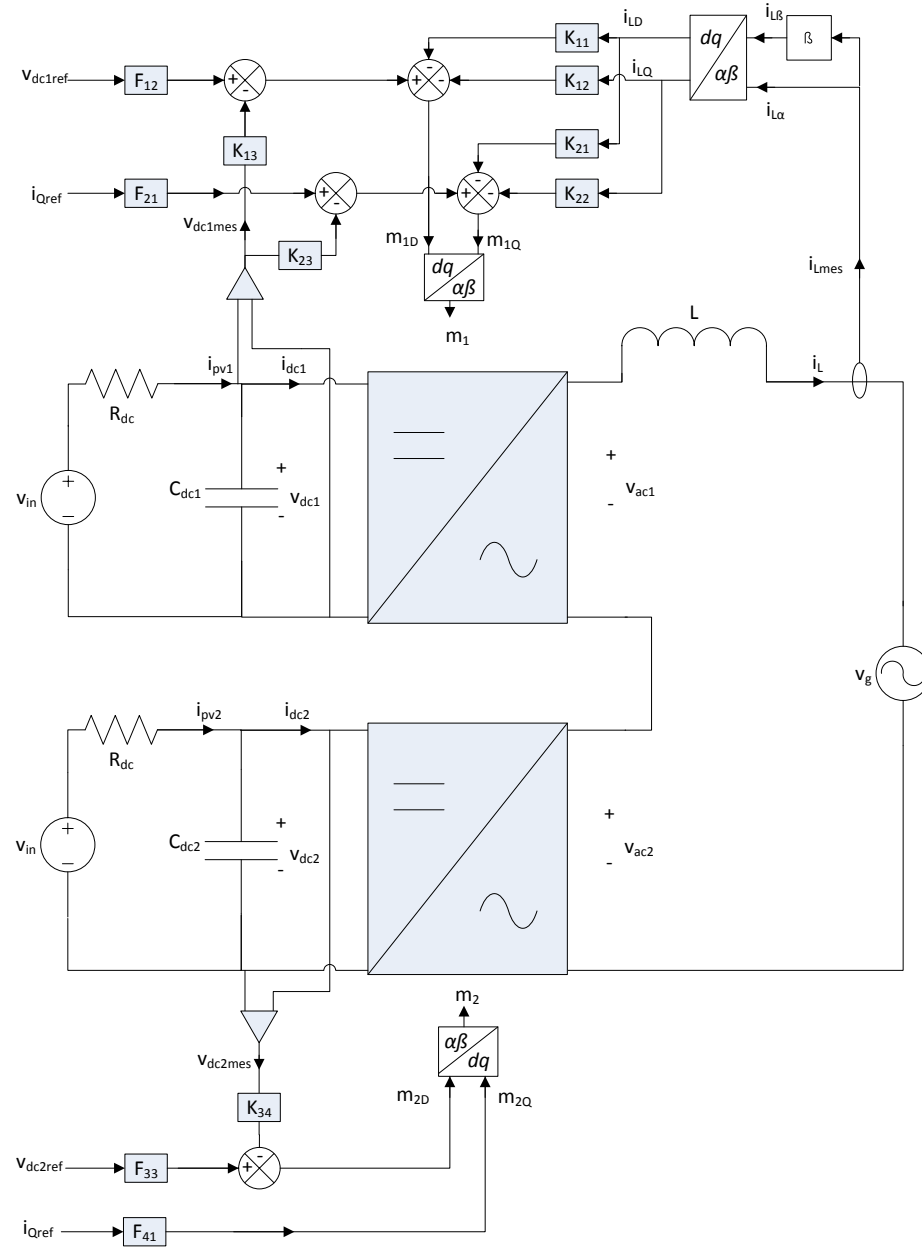


Figure 3.6: IM system with controller.

CHAPTER 4: SIMULATION AND RESULTS

4.1 Introduction

The main objective of this chapter is to corroborate the mathematical formulation and analysis for the distributed control scheme of IM presented in the previous chapter, with simulation test results. Section 4.2 outlines the simulation setup used for testing a two SM system of IM. The results and discussions are then presented in Section 4.3 under symmetric operation and asymmetric conditions like shading on one SM and grid disturbance.

4.2 Simulation Setup

The model is created in Simulink as shown in Figure 4.1. The simulation is setup for a discrete time step of $0.1 \mu\text{s}$ (10 MHz), which is 100 times the switching frequency ($f_{sw} = 100 \text{ KHz}$). As mentioned in the previous chapter, PV is emulated using a voltage source with a resistor. The switching model of the full bridge, consisting of MOSFETs is used. At the output of each SM, the LC filter is used and the series is connected to the grid through an inductor. The grid is emulated using a controlled voltage source fed by a sine wave.

The top string member (SM1) is controlling the string current and its own input power while the bottom string member (SM2) is controlling only its own power and producing the required output voltage. As shown in Figure 4.1, the controller for SM1 consists of an integrator which acts on the error of measured DC voltage and the output (AC current peak magnitude) goes to a Peak Current Controller block (PCC), which generates its PWM. Similarly, for SM2, the controller consists of the just the integrator block, which generates the modulation index for the Unipolar PWM

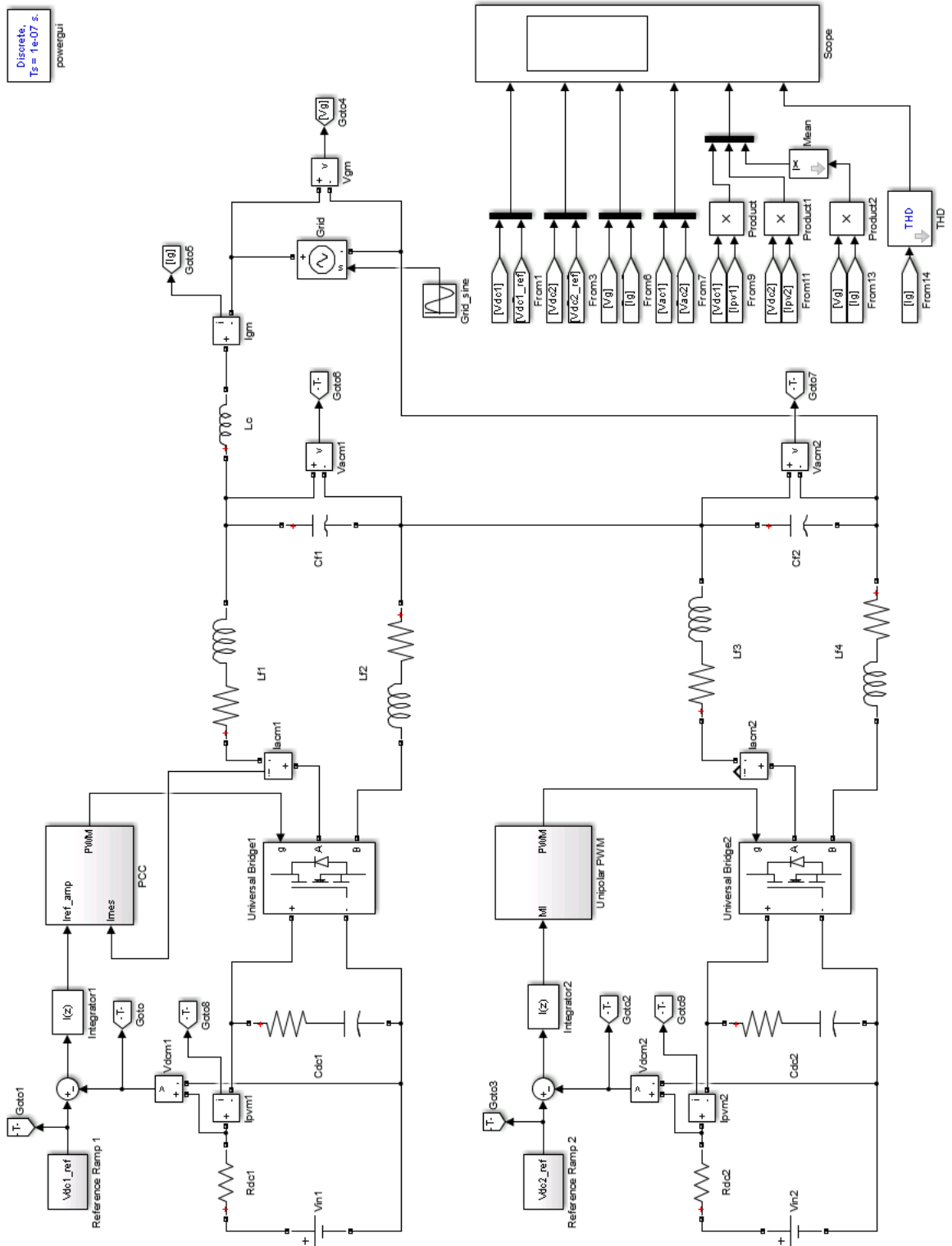


Figure 4.1: Simulink model of IM with controller.

generator.

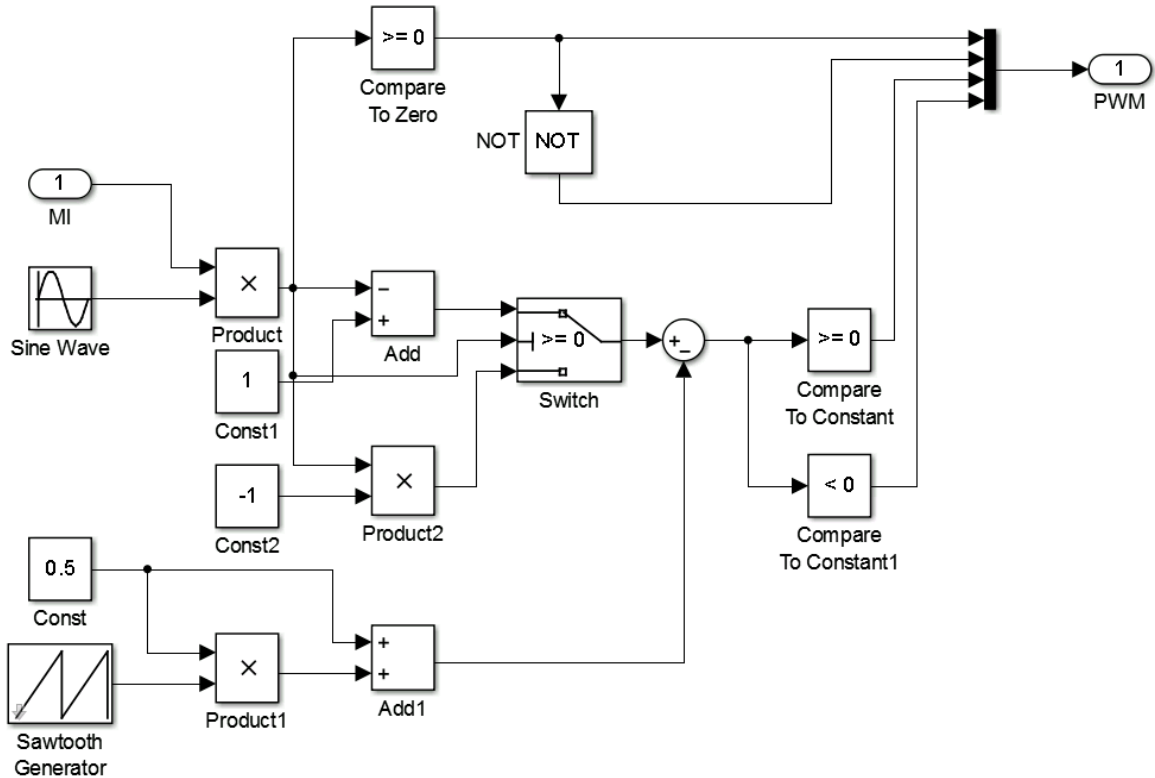


Figure 4.2: Simulink model of unipolar PWM generator.

The unipolar PWM generator details are shown in Figure 4.2. The modulation index is first multiplied by grid synchronized sine. The switching signals for the slow switching leg (60 Hz) are obtained by determining if the sine wave is in positive half or negative half. The signal for the top switch corresponds to the sign of sine while the bottom switch signal is its complementary. The signals for fast leg are determined by the sine-triangle method i.e. by comparing a sawtooth wave with the reference modulation index sine wave. The modulation function is different for different half of the sine wave and thus the switch. Based on the slow switch signals selected, the modulation functions for the fast leg top and bottom switch are $1 - \sin(\omega t)$ and $-\sin(\omega t)$.

The PCC block details are shown in Figure 4.3. The reference for PCC is generated by multiplying the amplitude reference with sine, which is synchronized with the grid.

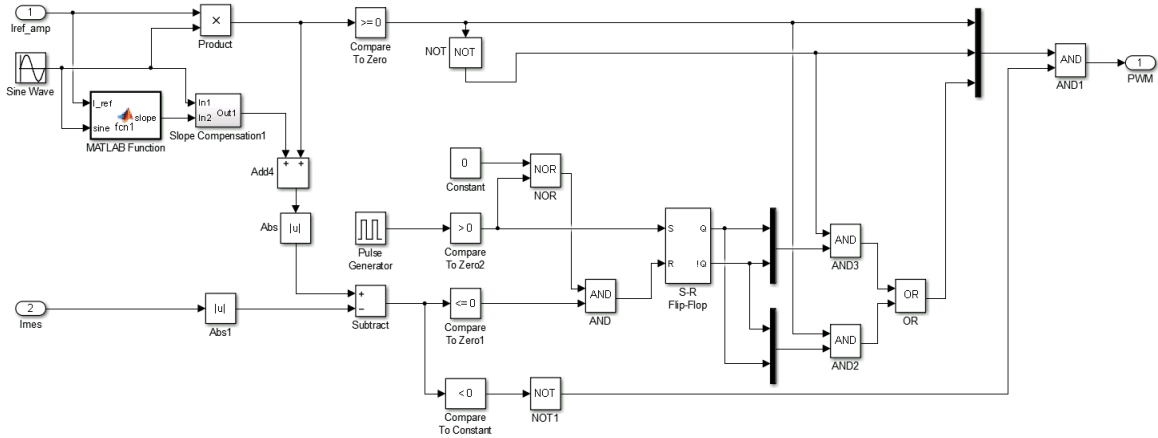


Figure 4.3: Simulink model of peak current controller.

An additional block of slope compensation is required so that duty cycles greater than 50%, which bring instability, are prevented. The slope compensation just subtracts a small ramp (at switching frequency) from the sinusoidal reference and the amplitude of this ramp changes dynamically with current, based on the MATLAB function block. The absolute value of the measured current is then compared with the absolute value of reference. This generates the reset signal for the SR-flip flop, the set signal for which is provided by a pulse generator at the switching frequency. Some additional logic using the NOR gate prevents the reset signal from being high for the initial 1% of the switching period. The outputs of the flip flop are gate signals for the fast switching leg of the H-bridge. The signals for the top and bottom switch are selected based on which switch of the slow leg is on. The switching signals for the slow leg are similar as explained for unipolar PWM. Additional logic is used to control the current near the zero crossings of the sine wave after peaks, because the current does not decrease even if fast side active switch is completely off (zero state). Thus, if current goes above reference then all the switches are opened.

The physical and controller parameters of the Simulink model are summarized in Tables 4.1 and 4.2. As it can be observed, the integrator gains are negative. This is because the current is inversely proportional to DC voltage, and decreasing the

voltage increases the current for our model. The sampling times of the integrators are 10 times slower than the switching frequency. This is acceptable because the inner loop current control is performed at switching frequency, as PCC is used.

Table 4.1: Physical parameters of simulink model.

V_{in1}, V_{in2}	39.7 V
R_{dc1}, R_{dc2}	0.9231 Ω
V_{dc1}, V_{dc2}	31.3 V
C_{dc1}, C_{dc2}	10 mF
$L_{f1}, L_{f2}, L_{f3}, L_{f4}$	150 μ H
C_{f1}, C_{f2}	1 μ F
L_c	50 μ H
V_g (amplitude of Grid_sine)	50 V
R_{pass} (resistance of passive elements)	10 $\mu\Omega$
R_{on} (On resistance of MOSFETs)	1 m Ω
f_{sw}	100 KHz

Table 4.2: Controller parameters of simulink model.

K_{I1} (Gain of Integrator 1)	-150
K_{I2} (Gain of Integrator 2)	-1
T_{s1} (Sampling time of Integrator 1)	100 μ s
T_{s2} (Sampling time of Integrator 2)	100 μ s

4.3 Simulation Results

4.3.1 Case 1: Symmetric Operation

In this case, both the SMs are operated with same parameters as indicated in Table 4.1. The DC voltage reference is reduced in steps of 2 V, every 0.2 s, for both the SMs, from the open circuit voltage V_{in} to the MPP voltage, as per the data sheet of a PV panel [25], of 31.3 V. Figures 4.4 and 4.5 show the change in reference voltage and the corresponding change in the DC voltage. The DC voltage has a 120 Hz ripple and

at MPP steady-state, the peak-to-peak is around 2.5 V (8%), which is in acceptable limits (for 98 % utilization [7]). This ripple may be completely eliminated by the full representation of IM with MFEC. The response of voltage controller is good, as after each transient, steady-state is reached in about 0.1 s.

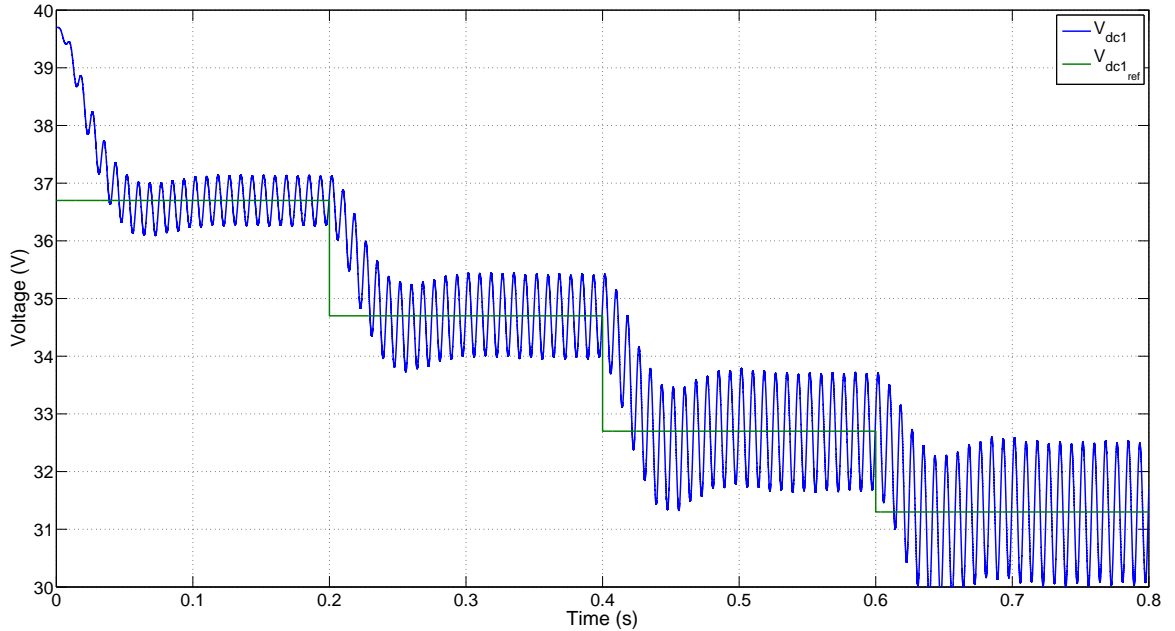


Figure 4.4: DC voltage and reference of SM1 for case 1: symmetrical ramping up to maximum power.

The grid side voltage and current are shown in Figure 4.6. It can be observed that the current ramps up as the DC voltage is ramped down in the previous figures. The response of the current controller is very fast and it can be verified from the figure as the peak envelope of the current exactly follows the slow changes in DC voltage. The current amplitude is about 22.786 A at MPP, as expected. The steady-state after reaching MPP, of the grid current and voltage between 0.75 s and 0.8 s, is shown in Figure 4.7. As it can be observed the current is exactly in phase with the grid voltage.

The THD of the current waveform as it ramps up to maximum power is shown in Figure 4.8. It can be observed that the THD is very high initially and decreases with increase in current. Also, at every transient in current reference (because of change

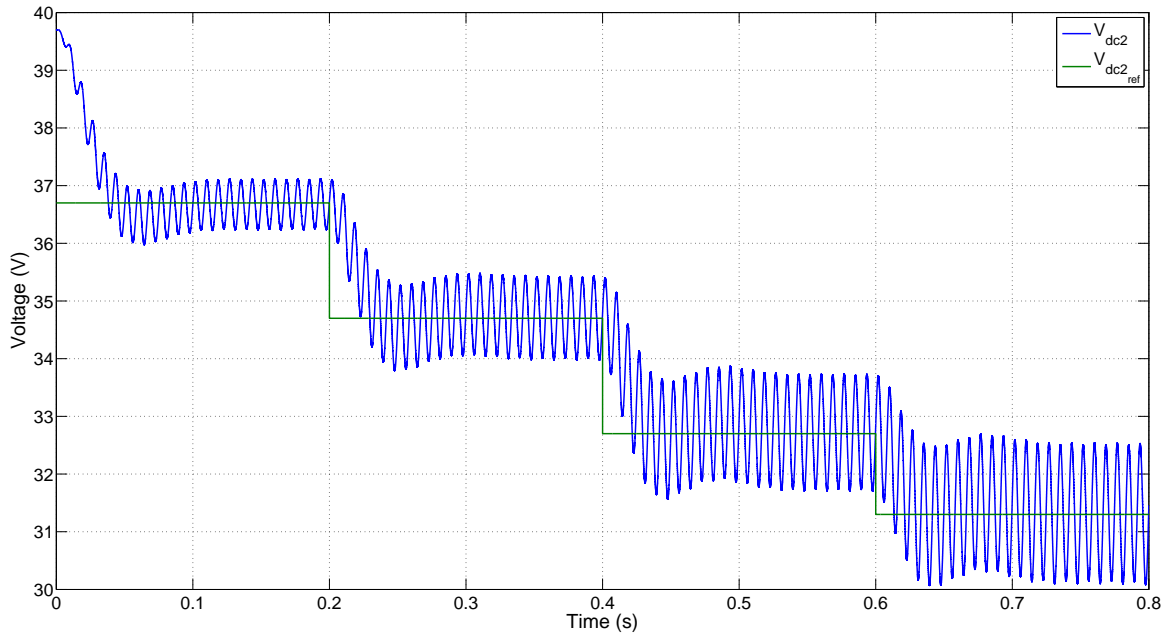


Figure 4.5: DC voltage and reference of SM2 for case 1: symmetrical ramping up to maximum power.

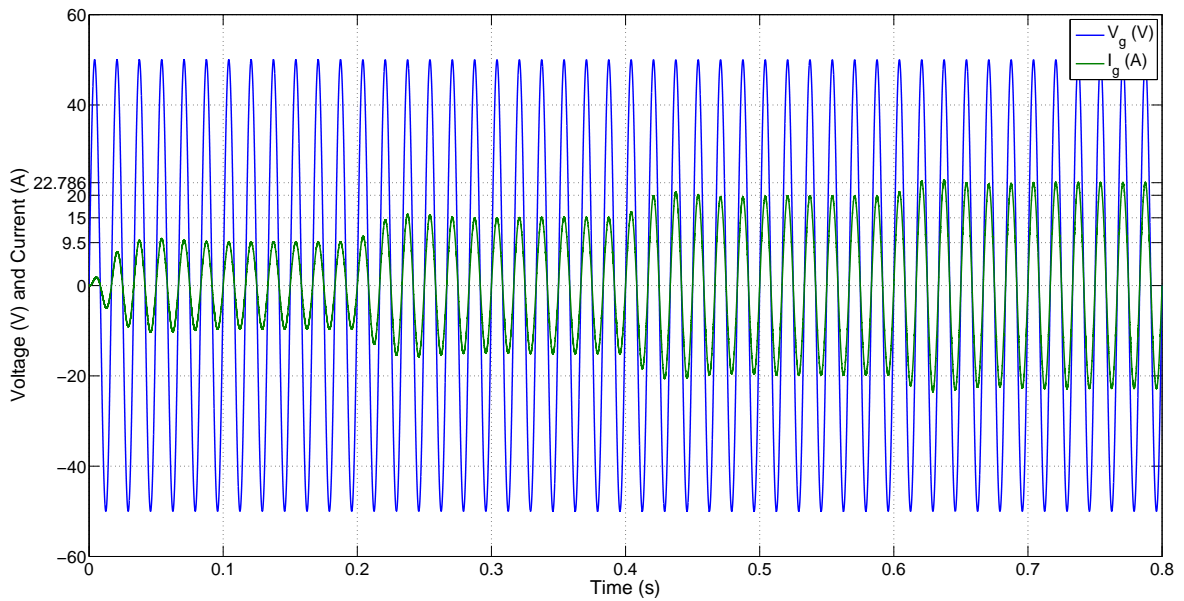


Figure 4.6: Grid voltage and current for case 1: symmetrical ramping up to maximum power.

in DC reference), the THD is higher and when it reaches the steady-state for that current value, the THD is much lower. The THD of the current at the maximum power steady-state is shown in Figure 4.9. It can be observed that the THD is much

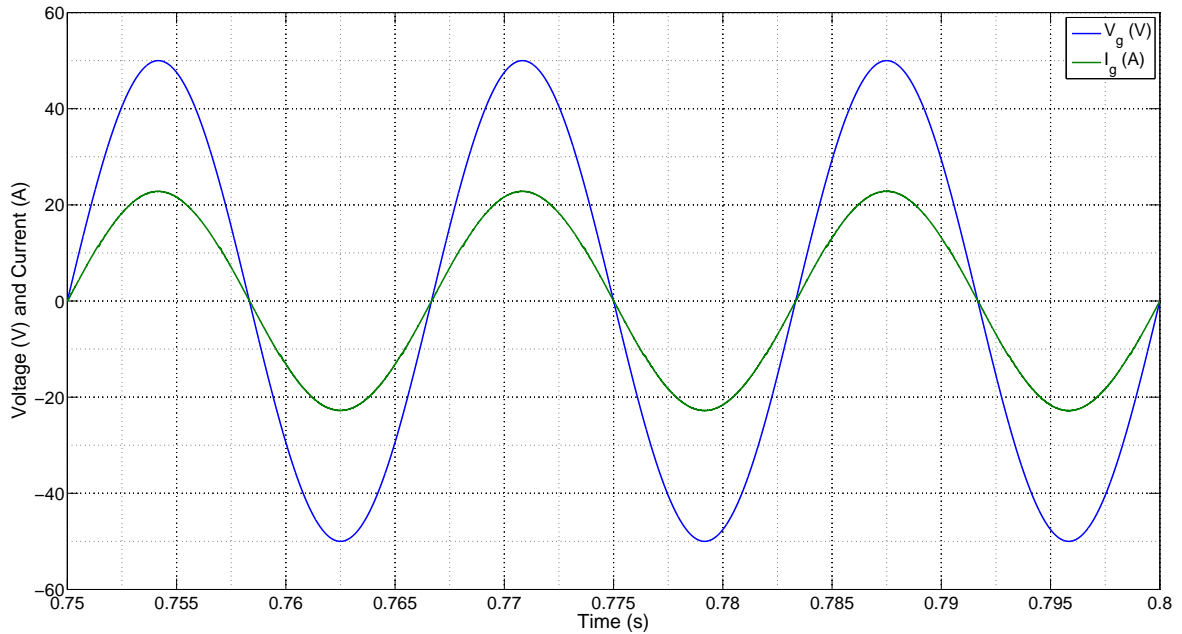


Figure 4.7: Grid voltage and current at MPP steady-state for case 1: symmetrical ramping up to maximum power.

lower than the Utility standards of 5%. It is around 0.62%.

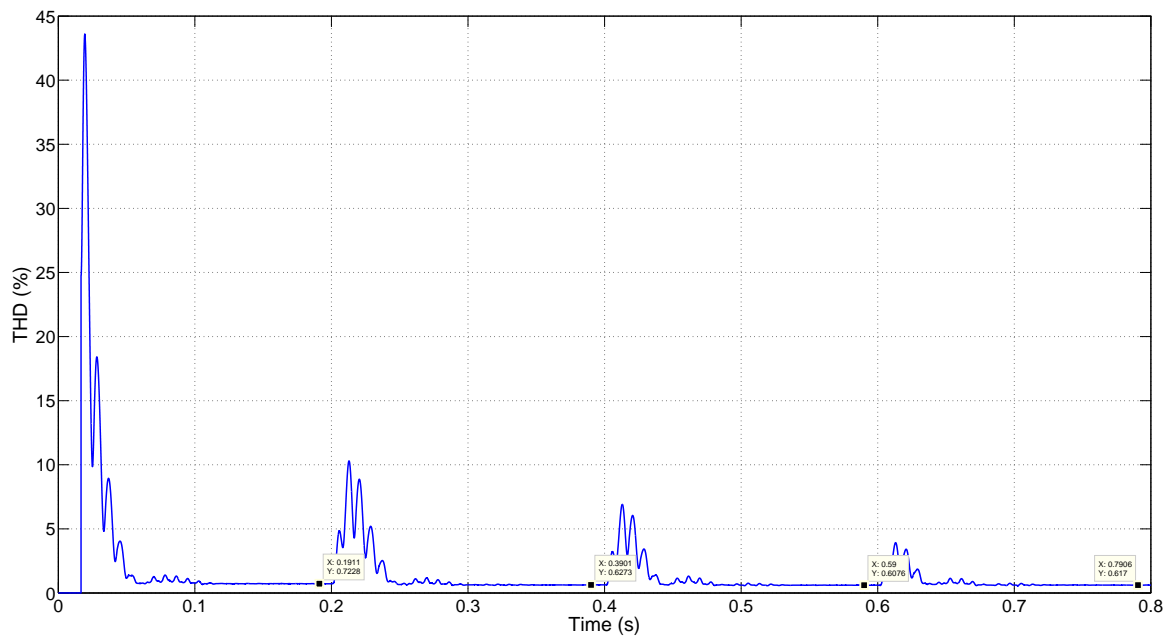


Figure 4.8: Grid current THD for case 1: symmetrical ramping up to maximum power.

The AC side voltages of the individual SMs are shown in Figure 4.10. It can be

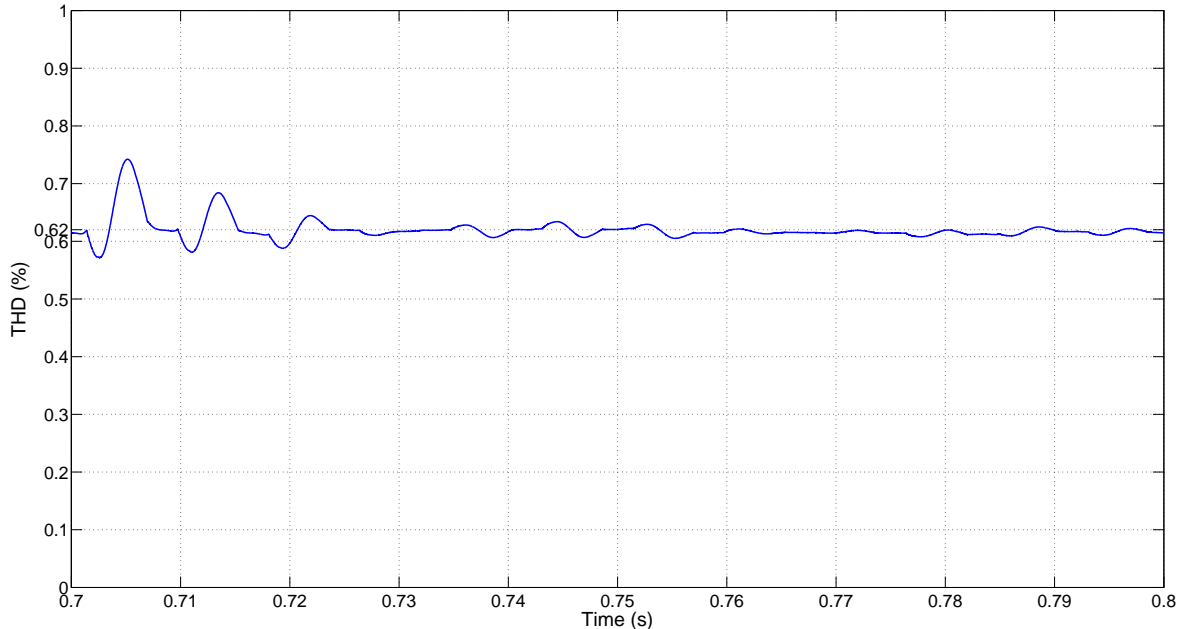


Figure 4.9: Grid current THD at MPP steady-state for case 1: symmetrical ramping up to maximum power.

observed that both voltages are almost equal and constant throughout the ramp-up to MPP i.e. the operation is symmetric and the grid voltage of 50 V is shared among the two SMs equally (around 25 V each).

The ramp in power, both the SMs DC power and the combined AC average power, is shown in Figure 4.11. Both SMs have equal power from input, of around 285 W, and the total AC power is about 567 W.

4.3.2 Case 2: Shading on SM2

In this case, power loss due to shading on SM2 is emulated as in the previous chapter Sub-Section 3.4.3, by reducing the V_{in2} as well as V_{dc2} to 36 V and 30 V respectively. After reaching MPP steady-state at 0.8 s, this change on DC side of SM2 is made at 0.9 s as shown in Figures 4.12 and 4.13. Here, it is assumed that the DC link voltage reference changes immediately as the input voltage changes, which is an extreme case. As it can be observed, the transient settles to steady-state for DC voltage of SM2 in about 0.2 s. This transient also affects the DC link voltage of SM1,

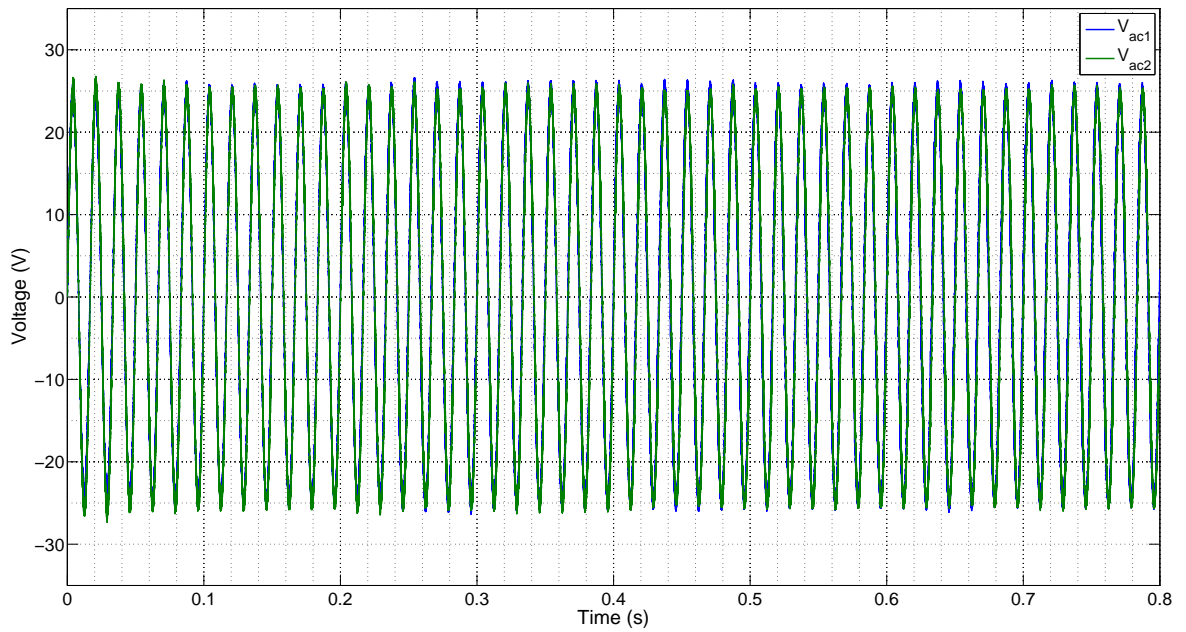


Figure 4.10: AC voltages of individual SMs for case 1: symmetrical ramping up to maximum power.

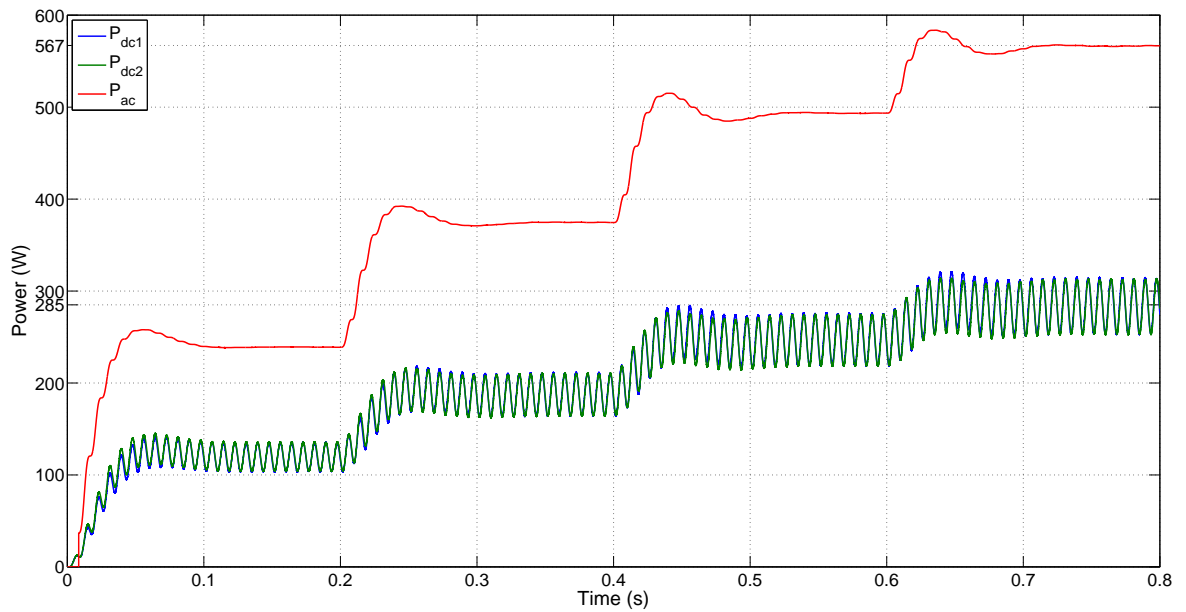


Figure 4.11: Power ramp-up for case 1: symmetrical ramping up to maximum power.

but it settles back in about 0.1 s.

The effect on the AC side or grid current can be seen in Figure 4.14. The current reduces with the reduction in power on SM2, to the expected value of about 19.19 A.

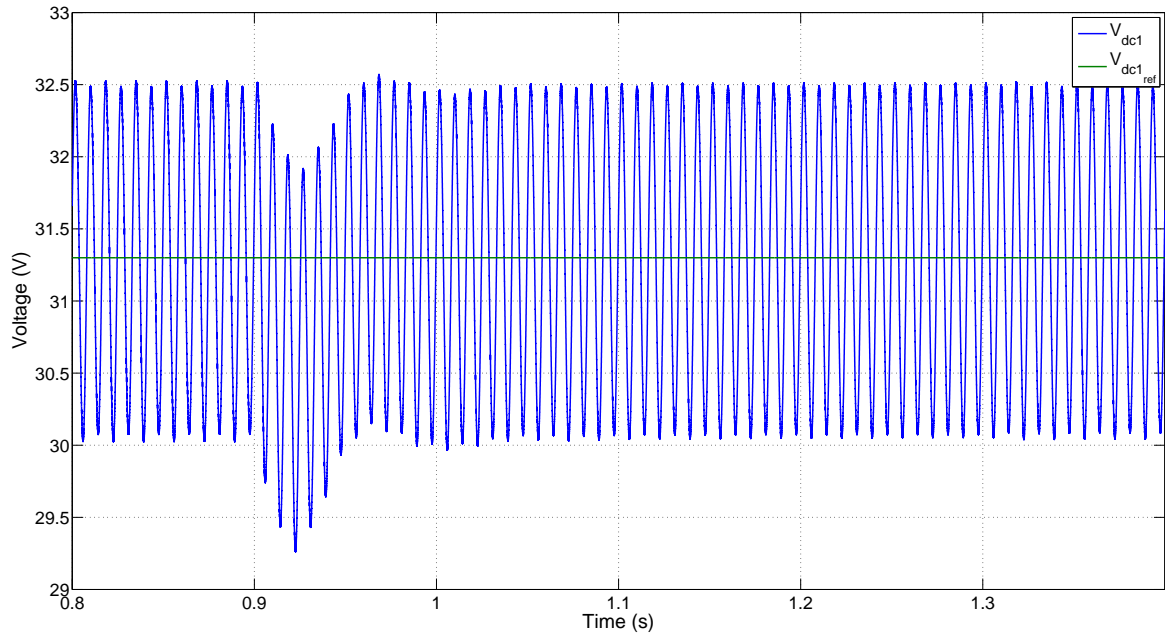


Figure 4.12: DC voltage and reference of SM1 for case 2: shading on SM2 at 0.9 s.

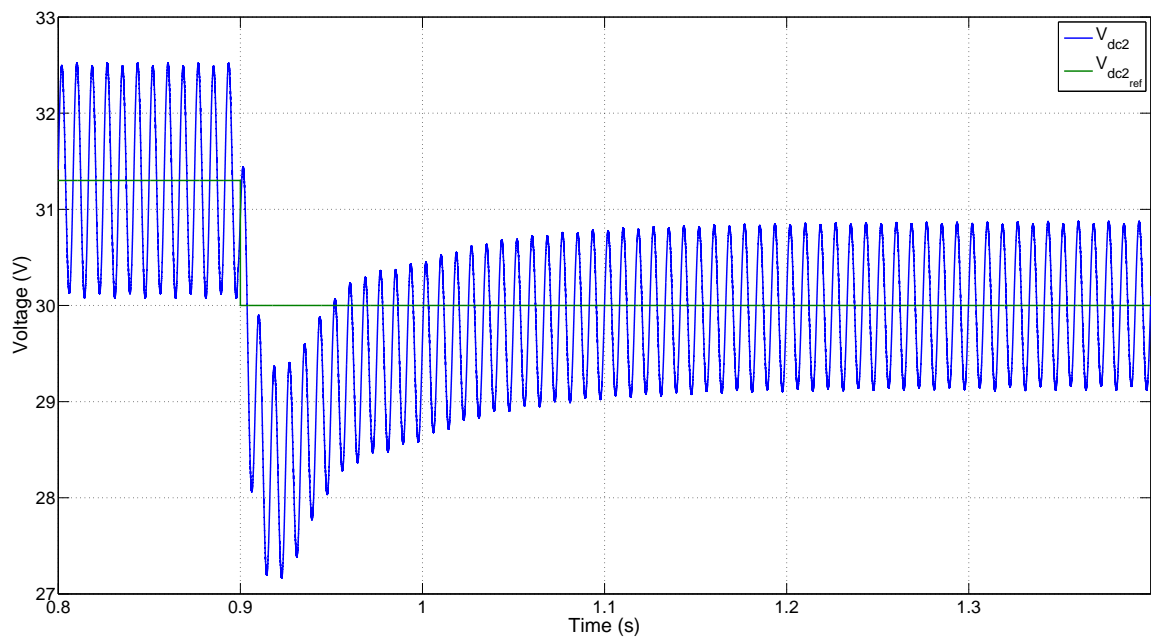


Figure 4.13: DC voltage and reference of SM2 for case 2: shading on SM2 at 0.9 s.

Also, it can be quantified from Figure 4.15 that the steady-state THD of the current is still very low, about 0.81%, but has increased from its previous (symmetric MPP) value.

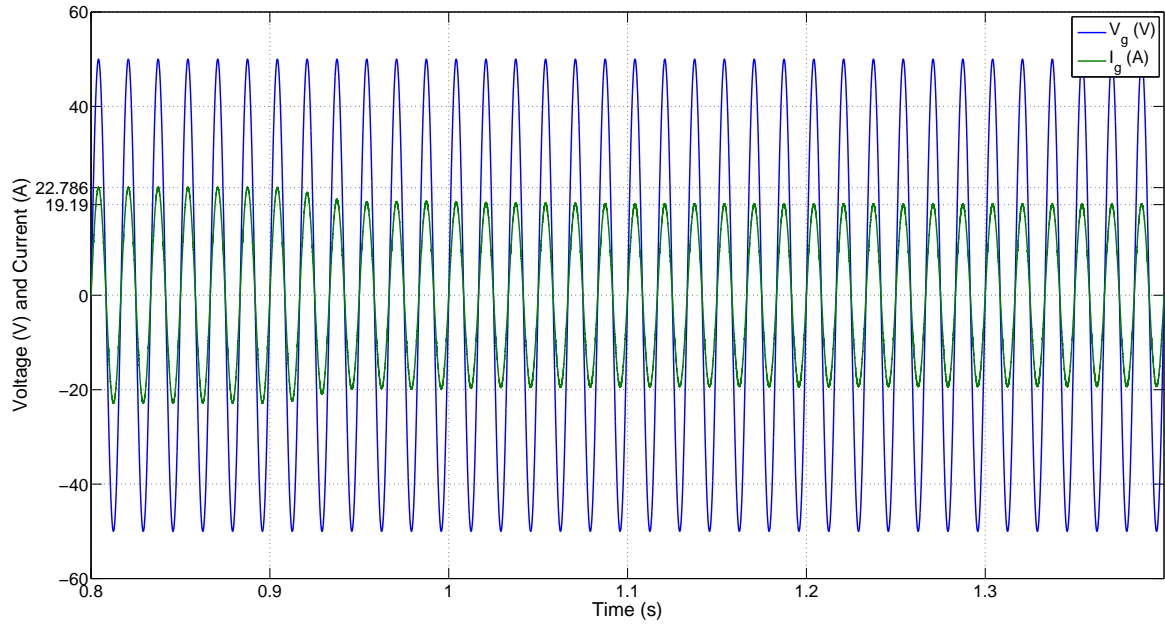


Figure 4.14: Grid voltage and current for case 2: shading on SM2 at 0.9 s.

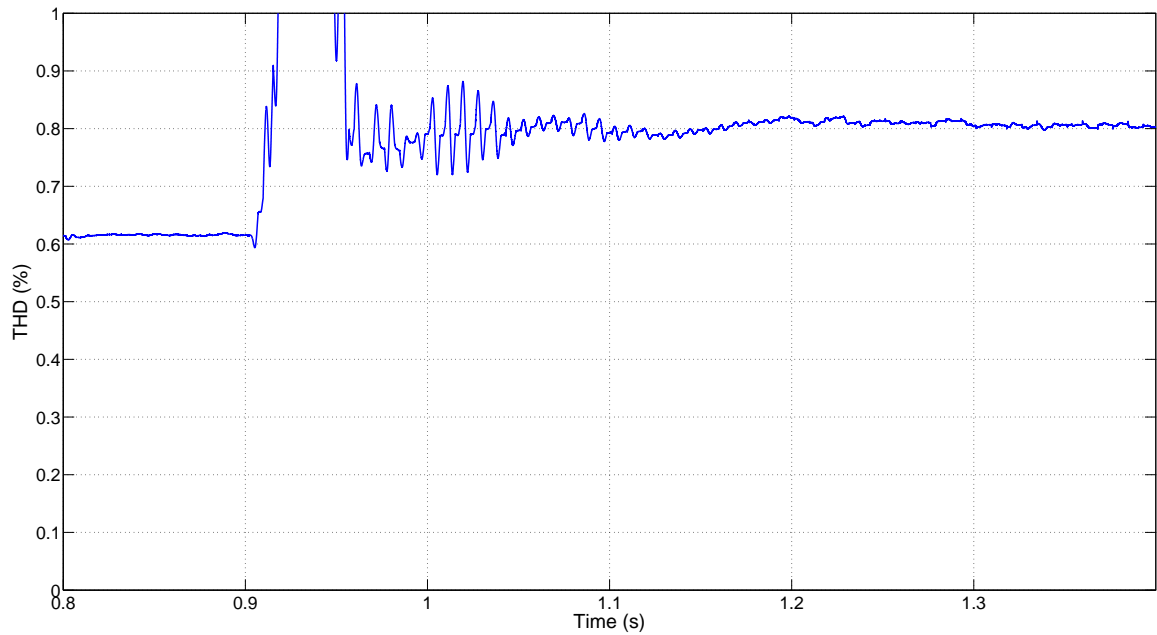


Figure 4.15: Grid current THD for case 2: shading on SM2 at 0.9 s.

Figure 4.16 shows the output voltages of both SMs. It can be observed that the AC voltage of SM1 increases to around 30 V (around 96% modulation), to maintain its own power balance and in-turn, compensates for the loss of SM2. The SM2 AC voltage is

reduced to about 20 V, and now it contributes less to the total grid voltage. Here, apart from acting as the current controller for the string, SM1 also acts (unintentionally) as the voltage compensator for the grid voltage.

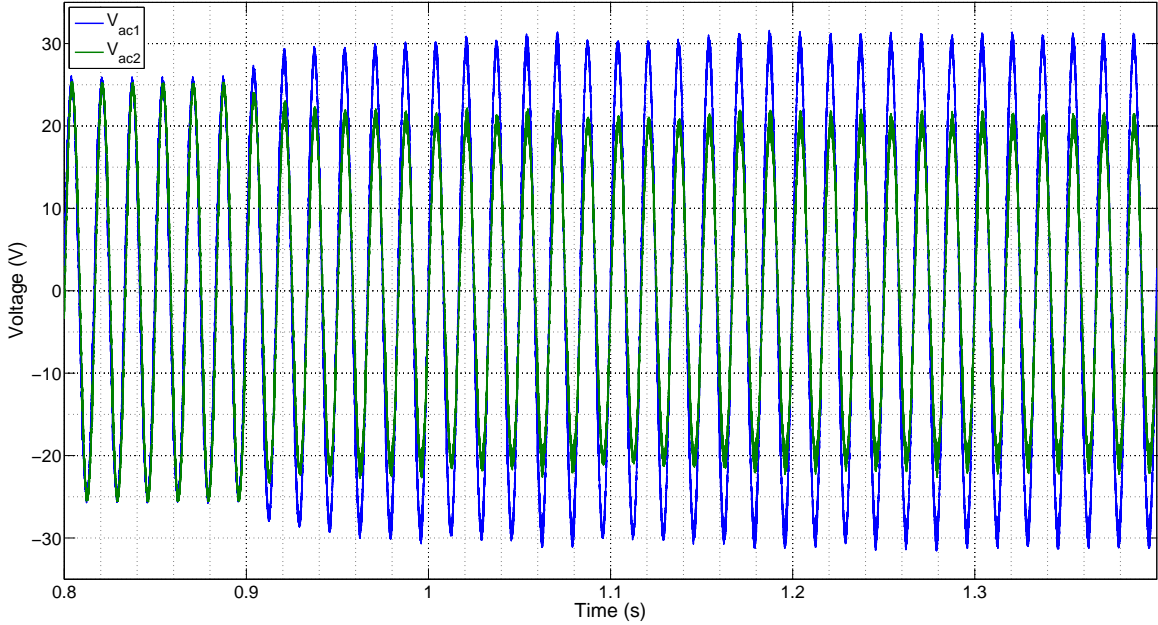


Figure 4.16: AC voltages of individual SMs for case 2: shading on SM2 at 0.9 s.

The power changes are shown in Figure 4.17. The power of SM2 gradually changes to about 195 W in 0.2 s. It can be observed that the average AC power also changes by the same amount (around 95 W). The DC power of SM1 gets affected slightly and only for a few cycles, as expected because of the change in V_{dc1} because of transient on SM2.

4.3.3 Case 3: Shading on SM1

In this case, shading on SM1 is emulated similarly as before. The V_{in1} is reduced to 36 V and V_{dc1} is reduced to 30 V. Figures 4.18 and 4.19 show the DC voltage change in SM1 and how it affects SM2. It can be observed that the transients are much higher (2-3 V) than in previous case. But settling time is similar, even though SM1 has shading it settles to steady-state in about 0.1 s while SM2 settles in 0.2 s.

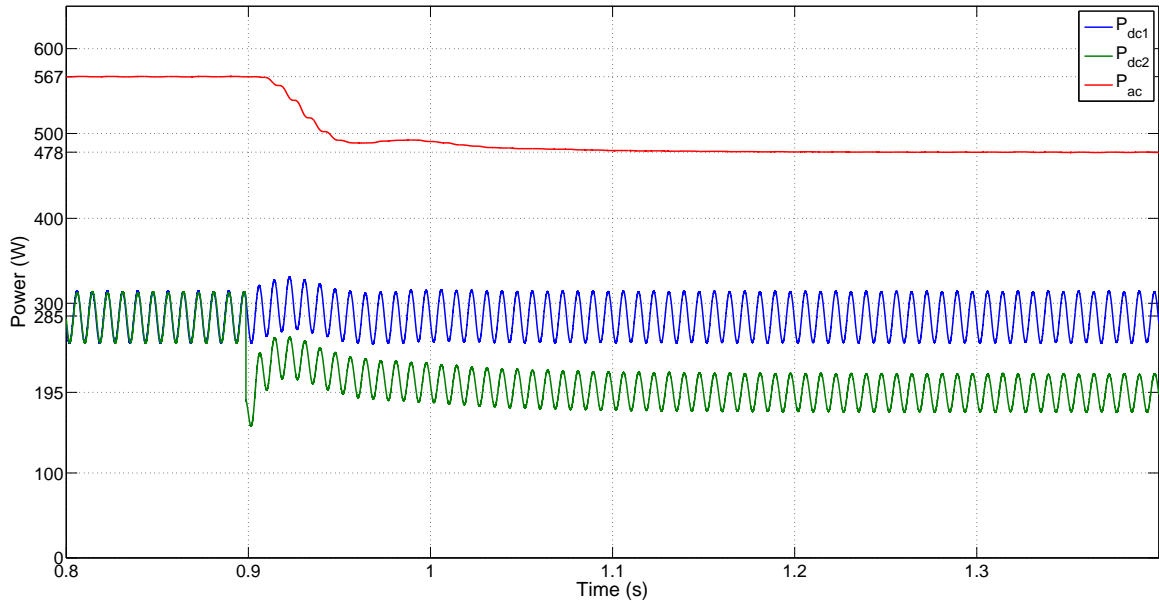


Figure 4.17: DC and AC power for case 2: shading on SM2 at 0.9 s.

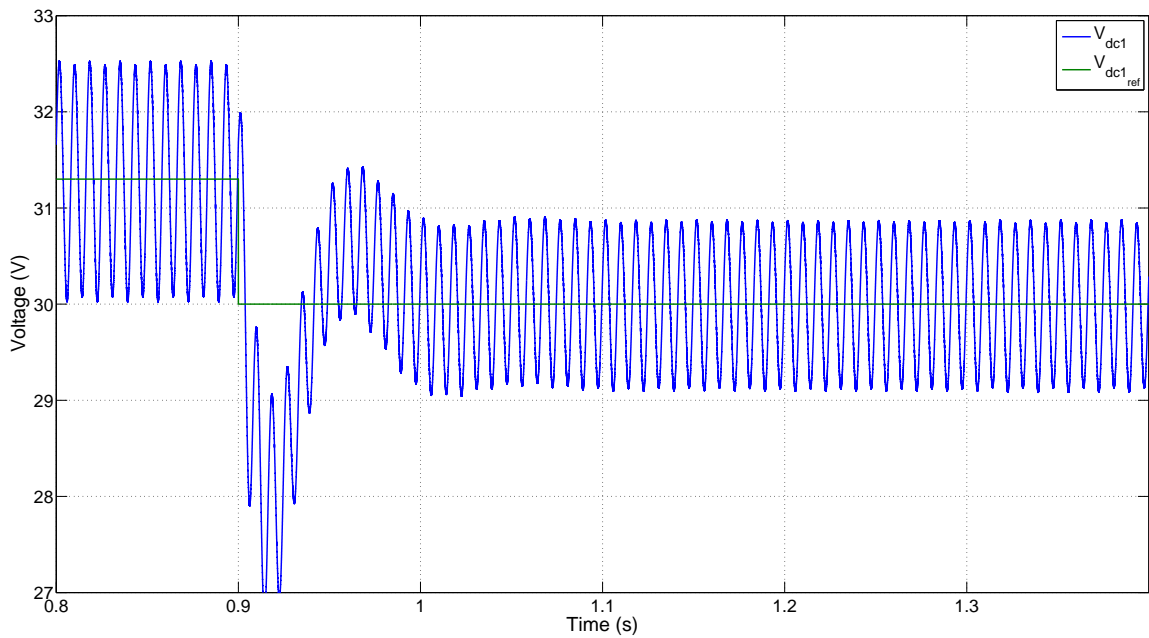


Figure 4.18: DC voltage and reference of SM1 for case 3: shading on SM1 at 0.9 s.

The effect on the AC side or grid current can be seen in Figure 4.20. The current reduces with the reduction in power on SM1, to the expected value of about 19.19 A as in the previous case with similar settling time. Also, it can be quantified from Figure 4.15 that the steady-state THD of the current is even lower than its previous

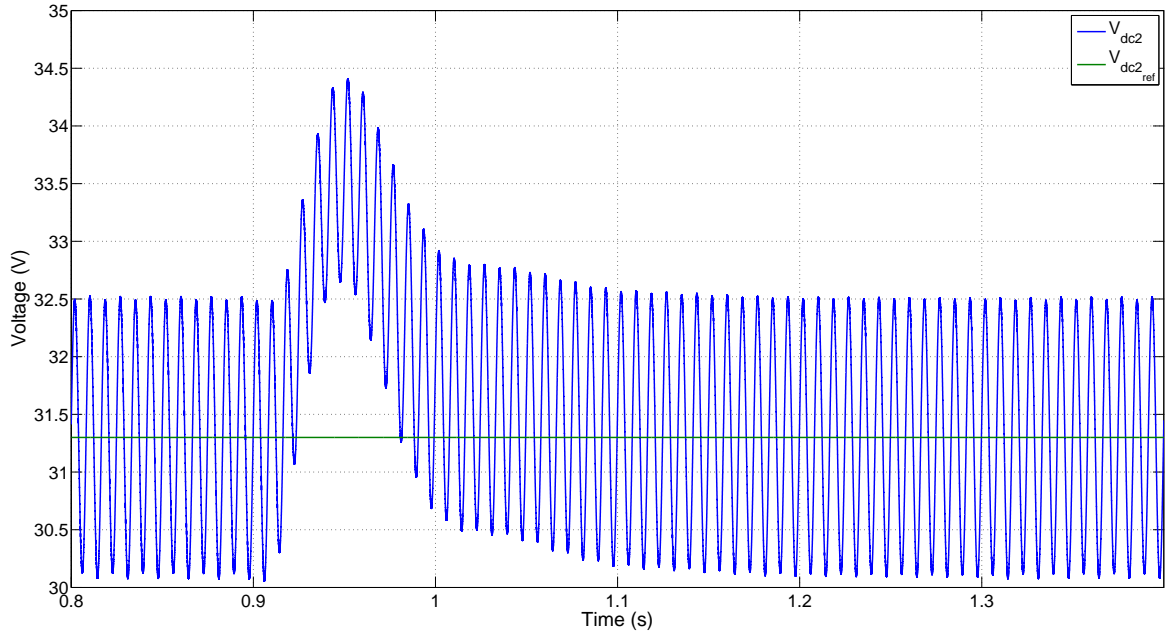


Figure 4.19: DC voltage and reference of SM2 for case 3: shading on SM1 at 0.9 s.

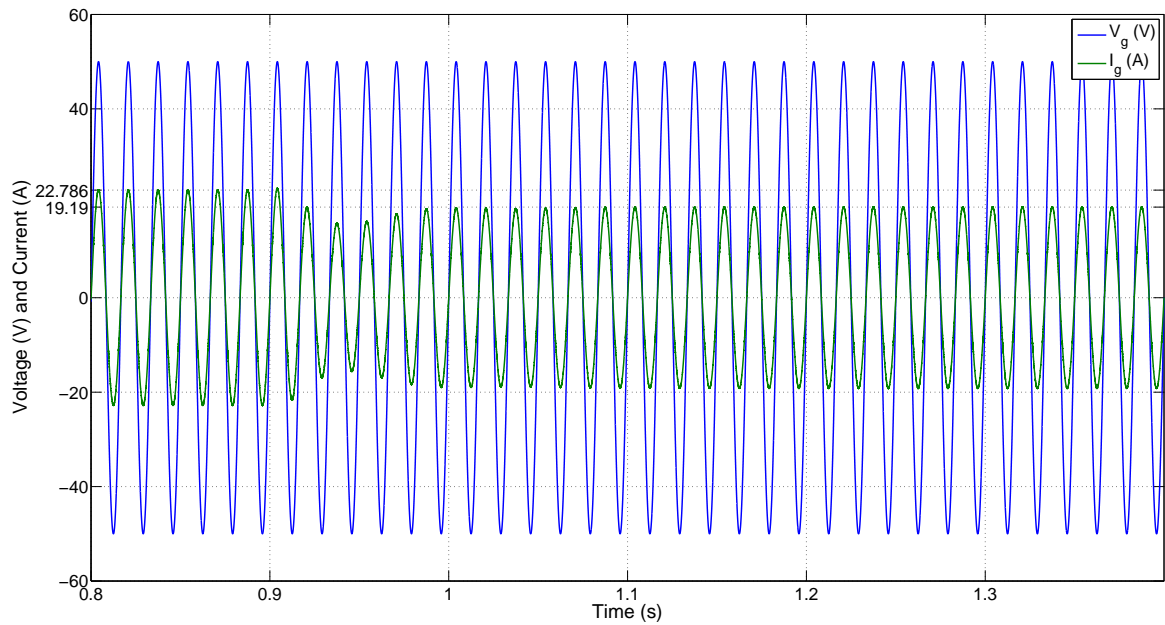


Figure 4.20: Grid voltage and current for case 3: shading on SM1 at 0.9 s.

(symmetric MPP) value, at about 0.54%.

The AC voltages of both SMs are shown in Figure 4.22. As it can be observed, the SM1 voltage reduces to about 20 V due to power loss, while the SM2 voltage increases

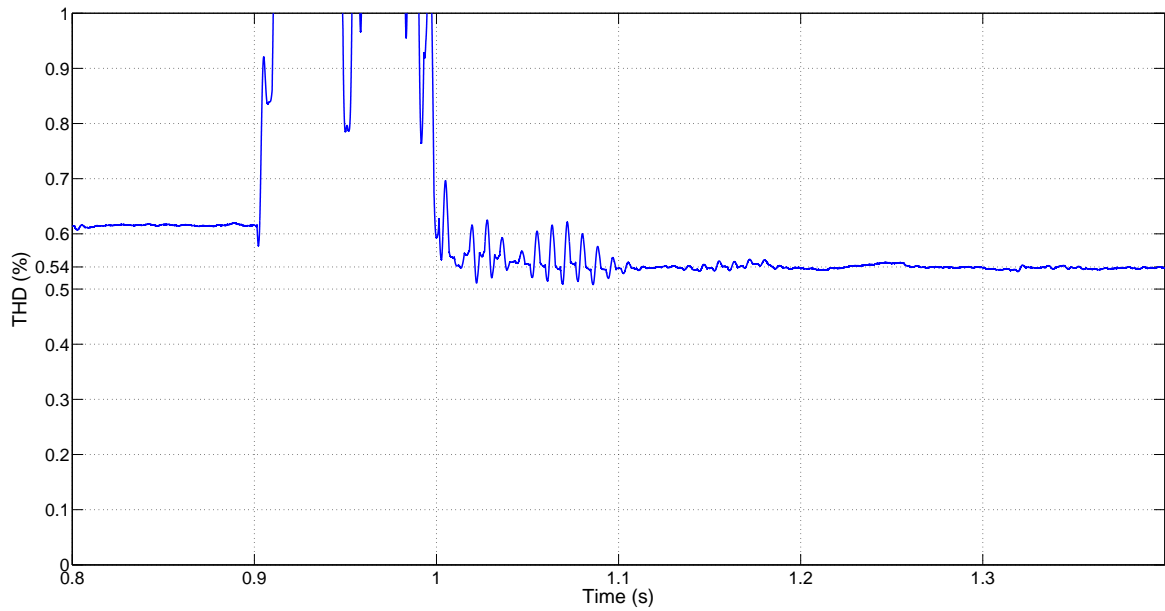


Figure 4.21: Grid current THD for case 3: shading on SM1 at 0.9 s.

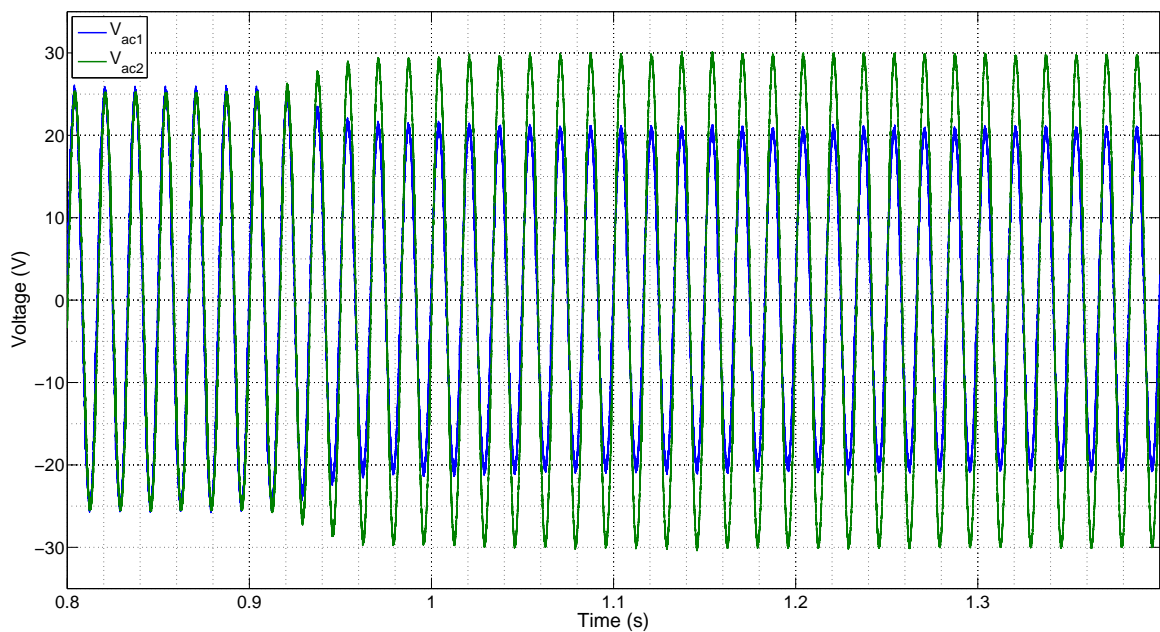


Figure 4.22: AC voltages of individual SMs for case 3: shading on SM1 at 0.9 s.

to about 30V to compensate for it. The variation of power is shown in Figure 4.23. SM1 power has decreased by around 90 W, and the total AC power has reduced by a similar amount to 478 W, as in the previous case. The effect to the DC power of SM2 is more than in previous case and it settles back in more time (around 0.1 s).

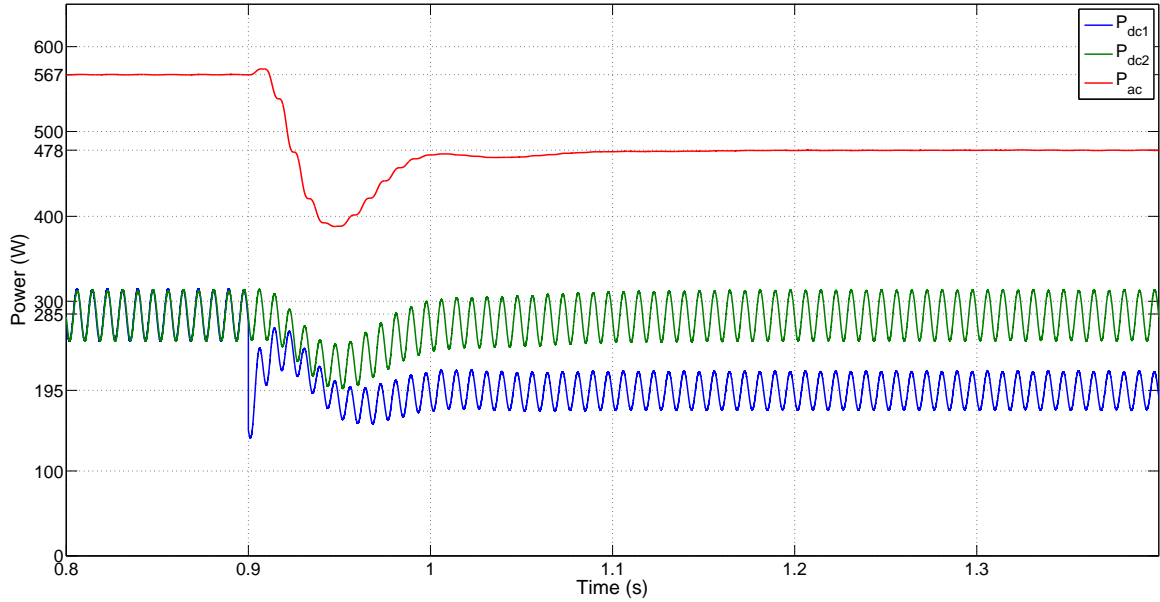


Figure 4.23: DC and AC power for case 3: shading on SM1 at 0.9 s.

4.3.4 Case 4: Grid Disturbance

In this case, a Grid disturbance is emulated by changing the peak of the grid voltage from 50 V to 55 V (10% change). After the MPP steady-state is reached at 0.8 s, this grid voltage change takes place at 0.9 s. Then, at 1.2 s, another grid disturbance, this time a huge change from 55 V to 45 V (18.18%), is added. These transients are shown in Figure 4.24, and the corresponding change in current, to maintain power balance, can also be seen.

The AC voltages of individual SMs are shown in Figure 4.25. At both the transients (0.9 s and 1.2 s), it can be observed that V_{ac1} of SM1 changes quickly according to the increase or reduction in grid voltage, thus acting as the voltage compensator. After a few cycles, the voltage contribution of both SMs becomes equal again.

This grid disturbance also affects the DC side of both SMs as shown in Figures 4.26 and 4.27. For SM1, the DC link voltage settles back in around 0.1 s after the first transient and about 0.2 s after the second transient. For SM2, the settling time is slightly more, and also the effect of the transient is more. While SM1 deviates from

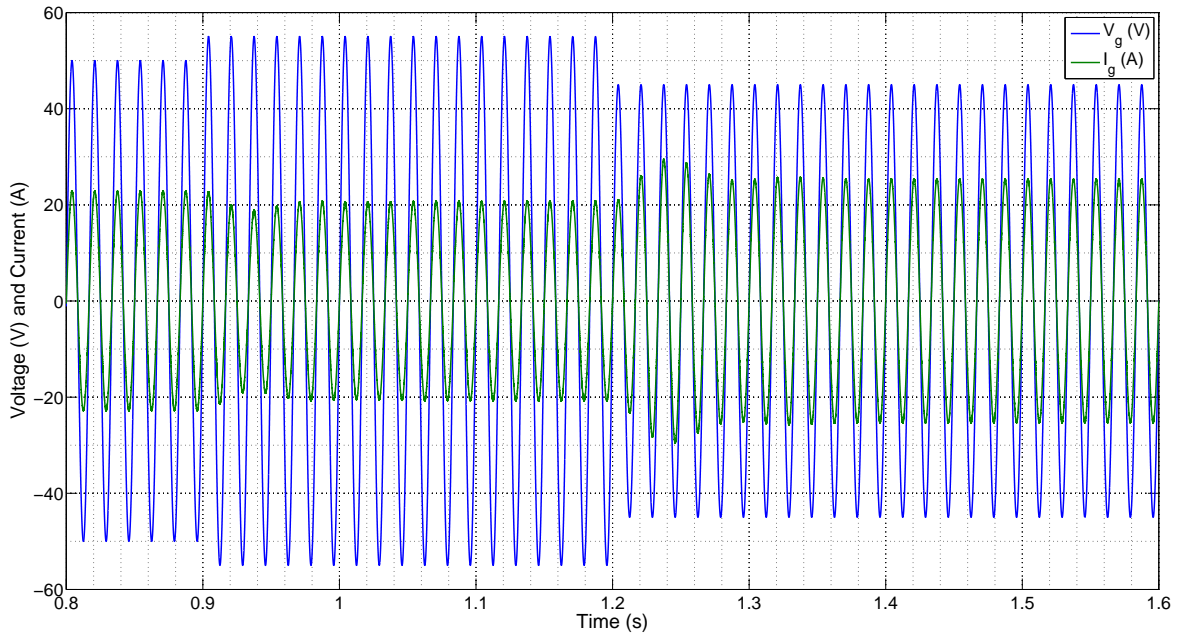


Figure 4.24: Grid voltage and current for case 4: grid disturbance - 10% at 0.9 s and 18.18% at 1.2 s.

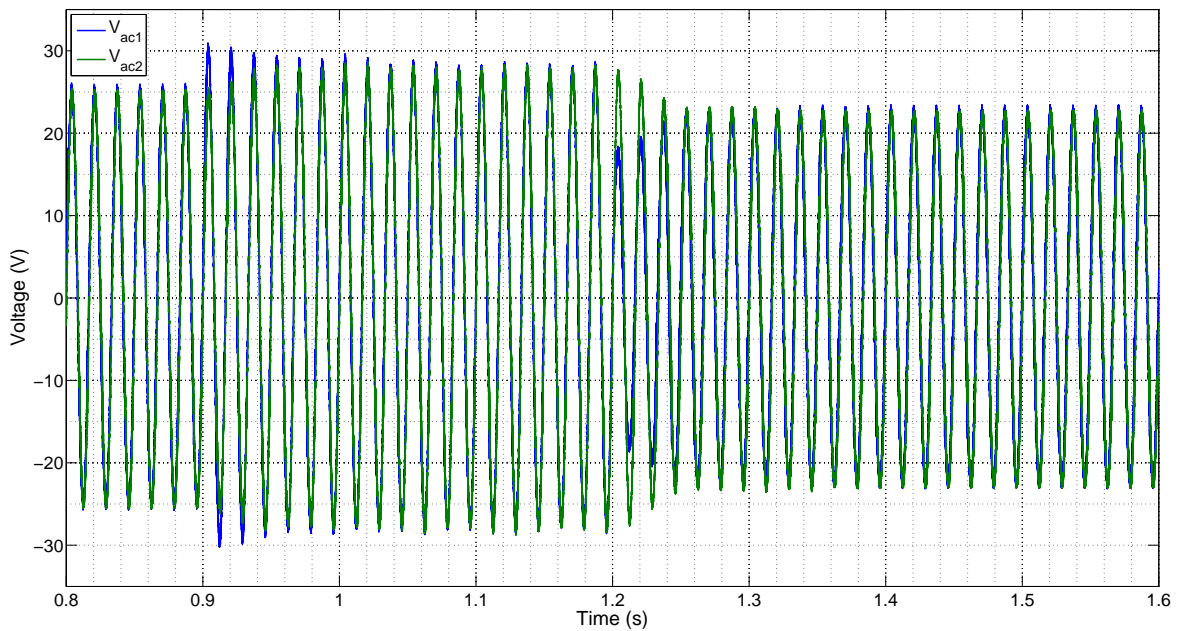


Figure 4.25: AC voltages of individual SMs for case 4: grid disturbance - 10% at 0.9 s and 18.18% at 1.2 s.

MPP voltage by approximately 1 V for first transient and 2 V for the second one, SM2 deviates by approximately 1.5 V and 2.5 V respectively.

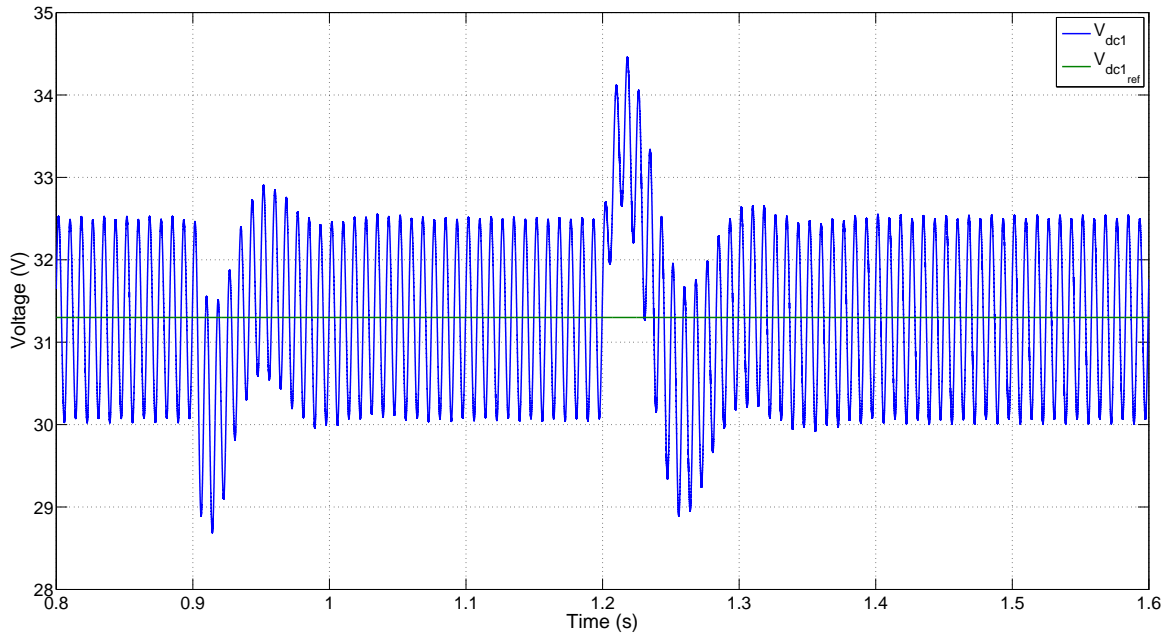


Figure 4.26: DC voltage and reference of SM1 for case 4: grid disturbance - 10% at 0.9 s and 18.18% at 1.2 s.

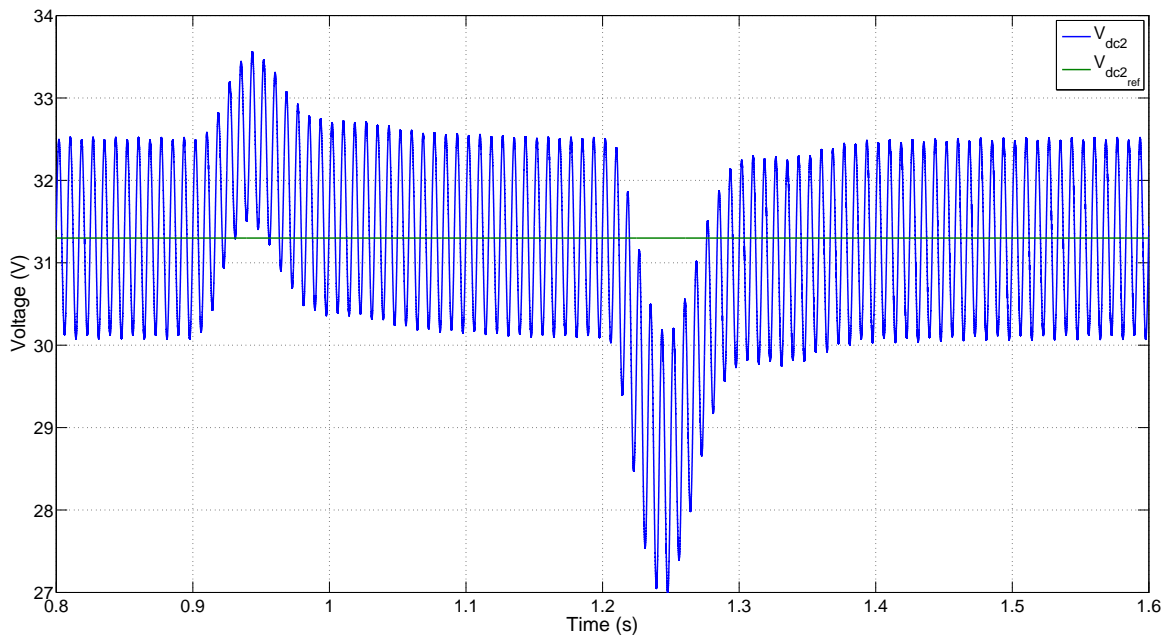


Figure 4.27: DC voltage and reference of SM2 for case 4: grid disturbance - 10% at 0.9 s and 18.18% at 1.2 s.

The power variations can be observed in Figure 4.28. At the first transient, the power increases slightly, then decreases and settles back. This is because, the SM1

voltage, to compensate for increase in grid voltage increases momentarily while the current is same. At the second transient, the power decreases first and then increases and settles back. This is because SM1 voltage first reduces along with the grid voltage while the current is same.

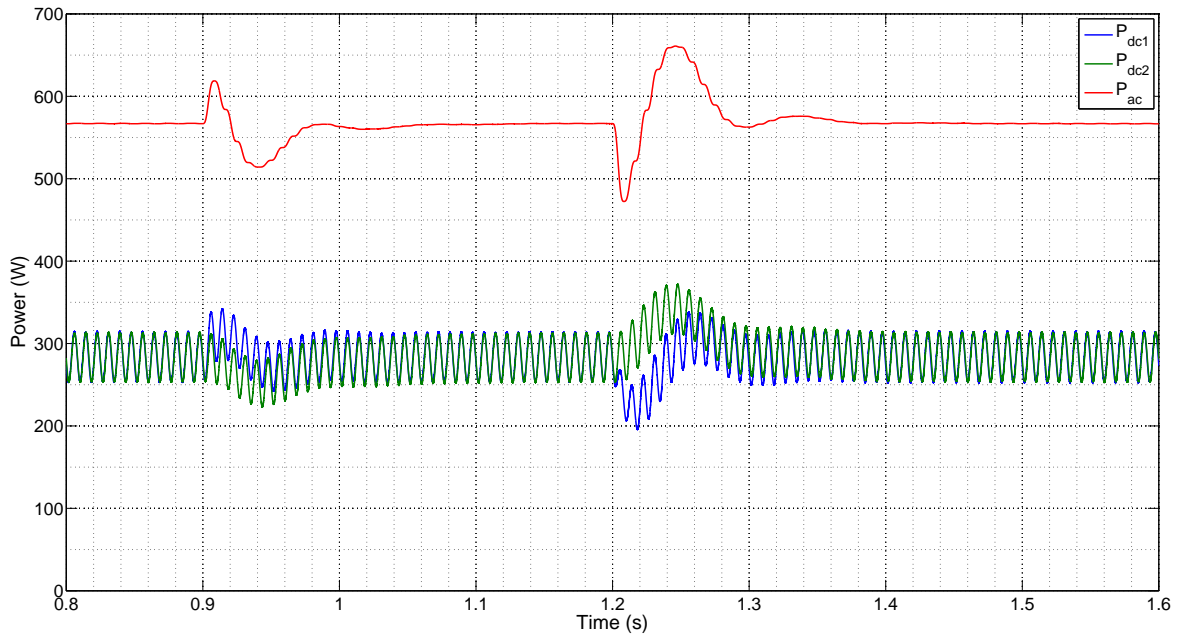


Figure 4.28: DC and AC power for case 4: grid disturbance - 10% at 0.9 s and 18.18% at 1.2 s.

The current THD variation with the transients is shown in Figure 4.29. When grid voltage decreases the THD increases to around 0.7% as the current magnitude reduces. But for the reduction in grid voltage the current increases and the current THD decreases to around 0.56%.

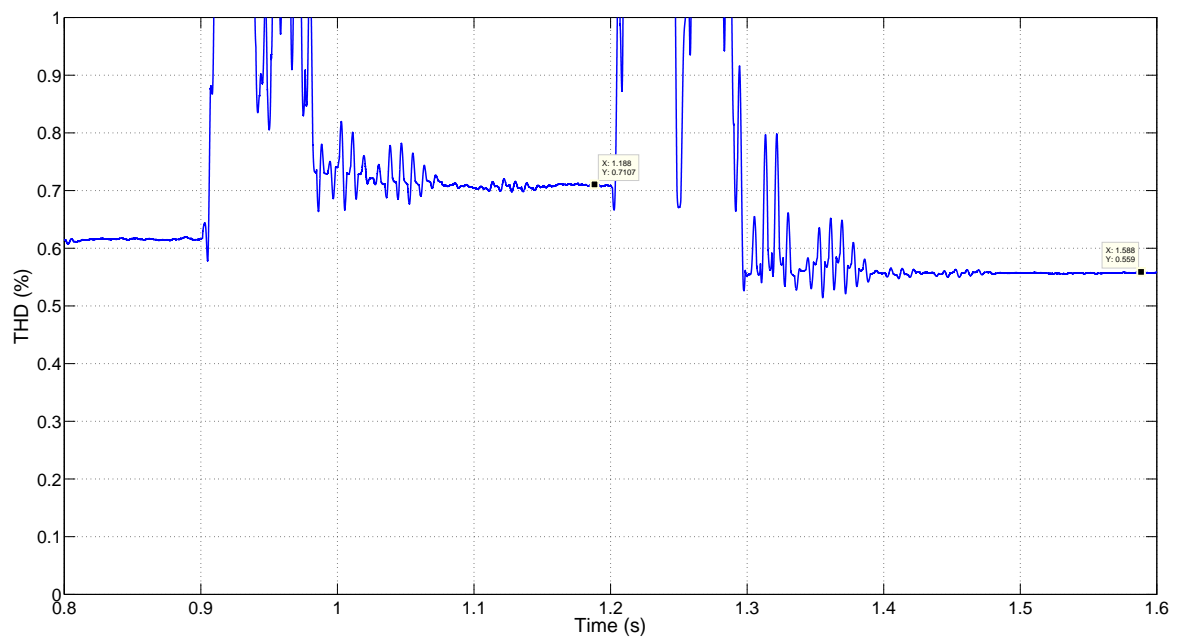


Figure 4.29: Grid current THD for case 4: grid disturbance - 10% at 0.9 s and 18.18% at 1.2 s.

CHAPTER 5: CONCLUSION

5.1 Summary

This thesis investigated the Inverter MoleculeTM architecture, and by deriving its mathematical model, designed, developed and analyzed a distributed control scheme. Since, the IM is AC stacked, the hypothesis was that each string member inverter can be controlled independently of any other string member information i.e. without any communication with other members, because the changes in power on any member will be inherently communicated by the AC current of the string to other members.

A linearized state space model for IM was derived and assessed for stability for a set of nominal operating points. Using state variable feedback, the hypothesized control scheme was designed and the closed-loop system thus obtained at the steady-state operating points, analyzed using step response, was found to be stable while also having the essential characteristics of a fast response and reference tracking. It was observed that it was not possible to completely decouple the two string members' DC side voltages because of the designed distributed control scheme, and a change in power of one string member affected the other member DC bus momentarily. Additional feedback of current for the SM2 can remove this coupling as well. It was also observed that for the controller designed, a set of asymmetric operating points also provided good step response characteristics with acceptable margin of error.

The designed control scheme was further developed using integrator compensator for the voltage control of all string members and a peak current controller for the CA, instead of just feedback and feedforward gains. This scheme was tested with a two string member switching model of IM in Simulink. Under symmetrical operating con-

ditions, both string members extracted maximum power with around 98% utilization (ripple of less than 8.5% on DC bus) and a sinusoidal current with unity power factor and 0.62% THD was supplied to the grid. The utilization can be increased by increasing the DC capacitor or adding another conversion stage like the IM proprietary MFEC stage. In the case of shading on the voltage controlling member, the DC bus of CA was slightly affected momentarily. In the case of similar shading on CA, the DC bus of the other member was affected more, and also for more time. In the case of grid disturbances, it was observed that the DC bus of both the string members get affected for some time. In all the asymmetric cases, it was demonstrated that both SMs track the reference at steady-state. It was also observed that the CA, under these transients, also acts as voltage compensator for the grid voltage. Also, from all the test cases it was observed that the CA, with the selected gains had much faster response than the other member.

5.2 Future Work

The decoupling and response times of the distributed control scheme presented here, can be further improved by adding current feedback for the string member that is not CA. Additional feedback or feedforward terms, like the output voltage of a string member, may also be included if required.

The control scheme presented here, can be extended, through analog or digital implementation, to a hardware implementation of IM. It can be tested with PV emulators and grid emulators or the actual PV modules and grid. For this, a separate MPPT controller will be required. A string of around 7 members can be used to connect to a 120 V grid. The peak current controller implementation can be analog, while the implementation of voltage controller can be digital, using a digital signal controller/processor (DSC/DSP). A ‘termination box’, at the connection to grid, which broadcasts the grid zero crossing information to all members, will also be required.

A D-Q current controller can also be used so that reactive power can be supplied

and controlled, instead of just multiplying the current reference with PLL output. To supply reactive power, only the phase of the modulation of CA may be changed or all the members can contribute to the change in phase. Such a phase change must be transmitted by the termination box.

The use of this distributed control scheme is not limited to the IM architecture, but can also be used for the CHB configuration. This is because, the state-of-the-art control scheme for CHB is not a truly distributed one.

REFERENCES

- [1] Electricity Data, U.S. Energy Information Administration (eia.gov/electricity/data.cfm).
- [2] U.S. Environmental Protection Agency (epa.gov/cleanenergy/energy-and-you/affect/water-discharge.html).
- [3] 2014 SunShot Initiative Portfolio Book (energy.gov/eere/sunshot/downloads/2014-sunshot-initiative-portfolio-book-tackling-challenges-solar-energy).
- [4] Progress Report: Advancing Solar Energy Across America (energy.gov/articles/progress-report-advancing-solar-energy-across-america).
- [5] Integrating Variable Renewable Energy: Challenges and Solutions (nrel.gov/docs/fy13osti/60451.pdf).
- [6] Bhowmik, Shibashis, "Systems and Methods for Solar Photovoltaic Energy Collection and Conversion," U.S. Utility application number 13/546868, July 11, 2012.
- [7] Kjaer, S.B.; Pedersen, J.K.; Blaabjerg, F., "A review of single-phase grid-connected inverters for photovoltaic modules," *Industry Applications, IEEE Transactions on* , vol.41, no.5, pp.1292,1306, Sept.-Oct. 2005.
- [8] Calais, M.; Myrzik, J.; Spooner, T.; Agelidis, V.G., "Inverters for single-phase grid connected photovoltaic systems-an overview," *Power Electronics Specialists Conference, 2002. pesc 02. 2002 IEEE 33rd Annual* , vol.4, no., pp.1995,2000, 2002.
- [9] Hassaine, L., OLias, E., Quintero, J. and Salas, V., (2014), "Overview of power inverter topologies and control structures for grid connected photovoltaic systems", *Renewable and Sustainable Energy Reviews*, 30, issue C, p. 796-807
- [10] IEEE Standard for Interconnecting Distributed Resources With Electric Power Systems, *IEEE Std. 1547*, 2003.
- [11] Ciobotaru, M.; Teodorescu, R.; Blaabjerg, F., "Control of single-stage single-phase PV inverter," *Power Electronics and Applications, 2005 European Conference on* , vol., no., pp.10 pp.,P.10, 0-0 0.
- [12] Fanbo He; Zhengming Zhao; Liqiang Yuan; Sizhao Lu, "A DC-link voltage control scheme for single-phase grid-connected PV inverters," *Energy Conversion Congress and Exposition (ECCE), 2011 IEEE* , vol., no., pp.3941,3945, 17-22 Sept. 2011.

- [13] Fanbo He; Zhengming Zhao; Ting Lu; Liqiang Yuan, "Predictive DC voltage control for three-phase grid-connected PV inverters based on energy balance modeling," *Power Electronics for Distributed Generation Systems (PEDG)*, 2010 2nd IEEE International Symposium on , vol., no., pp.516,519, 16-18 June 2010.
- [14] Meza, C.; Negroni, J.J.; Biel, D.; Guinjoan, F., "Energy-Balance Modeling and Discrete Control for Single-Phase Grid-Connected PV Central Inverters," *Industrial Electronics, IEEE Transactions on* , vol.55, no.7, pp.2734,2743, July 2008.
- [15] Kotsopoulos, A.; Duarte, J.L.; Hendrix, M.A.M., "Predictive DC voltage control of single-phase PV inverters with small DC link capacitance," *Industrial Electronics, 2003. ISIE '03. 2003 IEEE International Symposium on* , vol.2, no., pp.793,797 vol. 2, 9-11 June 2003.
- [16] Golestan, S.; Monfared, M.; Guerrero, J.M.; Joorabian, M., "A D-Q synchronous frame controller for single-phase inverters," *Power Electronics, Drive Systems and Technologies Conference (PEDSTC)*, 2011 2nd , vol., no., pp.317,323, 16-17 Feb. 2011.
- [17] Miranda, U.A.; Rolim, L.G.B.; Aredes, M., "A DQ Synchronous Reference Frame Current Control for Single-Phase Converters," *Power Electronics Specialists Conference, 2005. PESC '05. IEEE 36th* , vol., no., pp.1377,1381, 16-16 June 2005.
- [18] Hanju Cha; Trung-Kien Vu; Jae-Eon Kim, "Design and control of Proportional-Resonant controller based Photovoltaic power conditioning system," *Energy Conversion Congress and Exposition, 2009. ECCE 2009. IEEE* , vol., no., pp.2198,2205, 20-24 Sept. 2009.
- [19] Feng Tian; Kasemsan, S.; Batarseh, I., "An Adaptive Slope Compensation for the Single-Stage Inverter With Peak Current-Mode Control," *Power Electronics, IEEE Transactions on* , vol.26, no.10, pp.2857,2862, Oct. 2011.
- [20] Malinowski, M.; Gopakumar, K.; Rodriguez, J.; Perez, M.A., "A Survey on Cascaded Multilevel Inverters," *Industrial Electronics, IEEE Transactions on* , vol.57, no.7, pp.2197,2206, July 2010.
- [21] Kouro, S.; Bin Wu; Moya, A.; Villanueva, E.; Correa, P.; Rodriguez, J., "Control of a cascaded H-bridge multilevel converter for grid connection of photovoltaic systems," *Industrial Electronics, 2009. IECON '09. 35th Annual Conference of IEEE* , vol., no., pp.3976,3982, 3-5 Nov. 2009.
- [22] Villanueva, E.; Correa, P.; Rodriguez, J.; Pacas, M., "Control of a Single-Phase Cascaded H-Bridge Multilevel Inverter for Grid-Connected Photovoltaic Systems," *Industrial Electronics, IEEE Transactions on* , vol.56, no.11, pp.4399,4406, Nov. 2009.

- [23] Bailu Xiao; Ke Shen; Jun Mei; Filho, F.; Tolbert, L.M., “Control of cascaded H-bridge multilevel inverter with individual MPPT for grid-connected photovoltaic generators,” Energy Conversion Congress and Exposition (ECCE), 2012 IEEE , vol., no., pp.3715,3721, 15-20 Sept. 2012.
- [24] Bailu Xiao; Lijun Hang; Jun Mei; Riley, C.; Tolbert, L.M.; Ozpineci, B., “Modular Cascaded H-Bridge Multilevel PV Inverter With Distributed MPPT for Grid-Connected Applications,” Industry Applications, IEEE Transactions on , vol.51, no.2, pp.1722,1731, March-April 2015.
- [25] PV panel specifications (www.solarworld-usa.com/products-and-services/sunmodule-solar-panels).
- [26] William L. Brogan. 1991. Modern Control Theory (3rd Ed.). Prentice-Hall, Inc., Upper Saddle River, NJ, USA.